

Spin, spin-orbit, and electron-electron interactions in mesoscopic systems*

Yuval Oreg^a, P. W. Brouwer^b, X. Waintal^b and
Bertrand I. Halperin^c

^a*Department of Condensed Matter Physics, Weizmann Institute of Science,
Rehovot 76100*

^b*Laboratory of Atomic and Solid State Physics, Cornell University, Ithaca, NY
14853-2501 USA*

^c*Lyman Laboratory of Physics, Harvard University, Cambridge MA 02138 USA*

Abstract

We review recent theoretical developments about the role of spins, electron-electron interactions, and spin-orbit coupling in metal nanoparticles and semiconductor quantum dots. For a closed system, in the absence of spin-orbit coupling or of an external magnetic field, electron-electron interactions make it possible to have ground states with spin $S > 1/2$. We review here a theoretical analysis which makes predictions for the probability of finding various values of spin S for an irregular particle in the limit where the number of electron is large but finite. We also present results for the probability distribution of the spacing between successive groundstate energies in such a particle.

In a metallic particle with strong spin-orbit interactions, for odd electron number, the groundstate has a Kramers' degeneracy, which is split linearly by a weak applied magnetic field. The splitting may be characterized by an effective g -tensor whose principal axes and eigenvalues vary from one level to another. Recent calculations have addressed the joint probability distribution, including the anisotropy, of the eigenvalues. The peculiar form of the spin-orbit coupling for a two-dimensional electron system in a GaAs heterostructure or quantum well leads to a strong suppression of spin-orbit effects when the electrons are confined in a small quantum dot. Spin-effects can be enhanced, however, in the presence of an applied magnetic field parallel to the layer, which may explain recent observations on fluctuations in the conductances through such dots.

We also discuss possible explanations for the experimental observations by Davidovic and Tinkham of a multiplet splitting of the lowest resonance in the tunneling conductance through a gold nano-particle.

*This article is slated to appear as a chapter in "Nano-Physics and Bio-Electronics", edited by T. Chakraborty, F. Peeters, and U. Sivan (to be published by Elsevier Co.).

1 Introduction

During the last two decades the fabrication technology of small conducting islands, known as *quantum dots*, using semiconductor heterostructures, sputtering of small metal grains and other methods have advanced so much that they can behave, under the right conditions, as *artificial atoms* [1]. In contrast to natural atoms, these artificial atoms do not have special symmetries, unless special experimental efforts are being performed[1].

The electron spin is responsible for a number of interesting effects in small chaotic conducting islands at low temperatures which are quite distinct from the role of spin in a bulk material. The role of spin is modified by electron-electron interactions in a way that has consequences for the distribution of the energy separations between ground states with different number of electrons, as well as for the probability of finding different spin quantum numbers at a fixed number of electrons. Other interesting effects are produced by spin-orbit coupling, which is important distribution of energy levels and wavefunctions in closed quantum dots and may modifies its properties, and which affects the conductance distribution for an ensemble of open quantum dots. The addition of source and drain leads, and in case of semiconductor heterostructures gates that control the charge on the dot, allows one to measure the properties of the dot-leads compound as a function of V , the difference between the potentials on the source and drain, and V_g , the potential on the gate lead.

In Sec. 2 of this paper we discuss a few effects of electron-electron interactions in a closed dot, with no spin-orbit coupling and no significant Zeeman field. The analysis reviewed in this section has been developed by a number of research groups in the last few years. We re-derive here an effective low energy Hamiltonian that was first discussed in Ref. [2] using renormalization group (RG) arguments. Then, we extend our studies [3] for the ground state spin of a quantum dot, and analyze its influence on the Coulomb blockade peak spacing that appear in the conductance as we sweep V_g at zero bias voltage, V . Further details, concerning the parameters of the effective model in actual systems and the relation of the effective model to other models, are given in the Appendices to the paper.

In Section 3, we give a brief review of recent work on the effects of spin-orbit coupling in metal nanoparticles and GaAs quantum dots. The reader will be referred to the literature for a fuller account.

In Section 4, we discuss a problem motivated by experimental observations of Davidovic and Tinkham [4] of a multiplet splitting of the *lowest* resonance in the tunneling differential conductance through a gold nanoparticle as a function of the source-drain potential, V . We consider two possible mechanisms

that may lead to effects of that type. The first is due to an almost degenerate ground state (Subsection 4.1) and the second due to a nonequilibrium phenomenon (Subsection 4.2). In Subsection 4.3 we compare these mechanisms, which both involve electron spin and/or electron-electron interaction in an essential way, and suggest experimental ways to distinguish between them.

2 Electron-Electron Interactions in a Closed Dot

When the shape of the dot is symmetric [1], a part of its single particle levels are degenerate, just like in an atom with a spherically symmetric potential. The exact electron many body configuration, which is set by the repulsive interaction between the electrons combined with the Pauli exclusion principle, is summarized in a set of rules, known as Hund’s rules. The first of them assert that a partially filled set of degenerate levels will have the maximal spin that is consistent with the exclusion principle. This happens because for a system of several electrons the “most antisymmetric” coordinate wave function has the largest spin. The most antisymmetric wave function minimizes the Coulomb repulsion between the electrons because it vanishes when there are two electrons at the same point. Strong spin-orbit interactions may change Hund’s rules.

To create symmetric dots, special (experimental) effort is necessary. Any generic dot, however, does not have any special symmetry and can be considered as a chaotic one, its single particle levels may assumed to be random, and are described by random matrix theory (RMT). Many theories have concentrated on the statistical properties of random levels and the way they can be used to understand chaotic dots in actual experiments, for review see Ref. [5]. The interactions between electrons in the dot and between them and the environment were commonly described by the so-called *constant interaction model*. In this model all the effects of interaction are cast into a single capacitance that describes the change in the energy of the system due to the dot’s charging.

This class of models was very successful in explaining and predicting experimental results as Coulomb peak height fluctuations, conductance fluctuations through an open dot and so on [5]. However, it fails to explain experiments measuring motion of peaks in magnetic field [6], distributions of Coulomb blockade peak spacing [7–10], and multiplets that appear in a single Coulomb blockade peak [4]. Motivated by the failure of the constant interaction model, a few models that extend it were suggested [2,3,11–13]. In Subsection 2.1 we derive, by integrating out fast degrees of freedom in the RG sense, an effective low-energy-Hamiltonian, \mathcal{H}_{eff} . This effective Hamiltonian, first discussed in Ref. [2], describes the properties of the quantum dot at energies smaller

than the Thouless energy E_{Th} of the system, which is inversely proportional to the time it takes to cross the dot along its largest dimension. We then show that a proper choice of parameters for \mathcal{H}_{eff} and its analysis reproduced other models for the effects of electron–electron interaction in quantum dots. Appendix A presents some details of the relation and equivalence of different models. Throughout this article we will neglect fluctuations of the interaction parameters, we discuss the limits of this approximation in Subsection 2.1.1.

In the process of averaging over the fast motion of the electrons in the Fermi sea, three channels of interaction appear: The direct/charging channel, the exchange/spin channel and the Cooper channel. The actual values of the parameters that describe these channels in \mathcal{H}_{eff} depend on the fast motion of electrons. We can have a richer situation when there are intermediate scales between the Fermi energy and the Thouless energy, *e.g.*: the inverse of the mean free time, τ , between elastic collisions with static impurities in diffusive systems. In Appendix B we find, using the Fermi-liquid-theory, the effective exchange interaction parameter for several three and two dimensional systems. Its dependance on electron density in two dimensional Si-MOSFET and AlGaAs ballistic heterostructures is estimated. Appendix C deals with the renormalization of the Cooper channel.

After a detailed discussion of the model in Subsection 2.1, we use it to analyze several physical quantities. In Subsection 2.2 we present an extended version of our study in Ref. [3] of the ground state spin configuration distribution. The following Subsection (Subsection 2.3) discusses the effects of spin fluctuations in the ground state on the Coulomb blockade peak distribution, (see also Ref. [12]). In Subsection 2.3.1 we compare some predictions of the theory with available experimental results [9,10]. We find that, although several features of the theory are observed in experiments, there is still disagreement between theory and experiment. We will discuss the possible causes for this discrepancy.

2.1 Effective Hamiltonian

To find properties, such as the ground state spin distribution of electrons in the dot in the presence of electron–electron interactions, we would like to describe them at low energy in a simple form. Ref. [2] shows that in the limit of large dots the effective Hamiltonian, at energies smaller than E_{Th} , is:

$$\mathcal{H}_{\text{eff}} = \sum_{\mu,s} \varepsilon_{\mu s} \psi_{\mu s}^{\dagger} \psi_{\mu s} + J_s \vec{S} \cdot \vec{S} + J_c T^{\dagger} T + U_c N^2. \quad (1)$$

Here, $N = \sum_{\mu,s=\uparrow,\downarrow} \psi_{\mu s}^{\dagger} \psi_{\mu s}$, $\vec{S} = \sum_{\mu,s,s'} \frac{1}{2} \psi_{\mu s}^{\dagger} \vec{\sigma}_{s,s'} \psi_{\mu s'}$ and $T = \sum_{\mu} \psi_{\mu\uparrow}^{\dagger} \psi_{\mu\downarrow}$. The μ sum runs over $M \equiv g = 2\pi E_{\text{Th}}/\Delta$ states. The symbol $\Delta = 1/(\nu\mathcal{V})$

denotes the average single particle level spacing in a dot of volume \mathcal{V} and thermodynamic density of states ν (per spin). Notice that in our notation Δ refers to the level spacing for a single spin state in the dot. In a dirty dot of length L and diffusive constant D , $E_{\text{Th}} = D/L^2$, while for a single dot we replace D by $\sim v_F L$.

The first term in (1) is universal: ε_μ is a single electron eigenenergy of a random matrix, and the operator $\psi_{\mu,s}^\dagger$ is the creation operator of an electron with spin S at an eigenstate μ of a random matrix. The set $\{\varepsilon_\mu\}$ depends on the symmetry of the problem. In the presence of time reversal symmetry the eigenenergies are taken from the Gaussian orthogonal ensemble (GOE, $\beta = 1$), and in the absence of time reversal symmetry from the Gaussian unitary ensemble (GUE, $\beta = 2$). When strong spin-orbit interactions are present they are taken from the Gaussian symplectic ensemble (GSE, $\beta = 4$)¹.

The direct Coulomb interaction constant U_c , the exchange constant J_s , and the interaction in the Cooper channel J_c depend on the specific system and the model one uses for the interaction. In addition, there are non universal corrections to Hamiltonian (1) that vanish, however, in the limit of $g \rightarrow \infty$. (See also in Subsection 2.1.1.) When the time reversal symmetry is broken the interaction in the Cooper channel vanishes. We will see below that even in the presence of time reversal symmetry the interaction in the Cooper channel is reduced due to a “screening” by fast electrons (see also Appendix C).

To understand what are the effective low energy interaction constants U_c , J_s , and J_c it is useful to describe the derivation of the effective Hamiltonian (1) in terms of a RG scheme. When the temperature decreases we integrate out progressively the fast motion of the electrons with energy far from the Fermi energy and find effective coupling constants in the direct (U_c), exchange (J_s) and Cooper (J_c) channels [14,15]. First, the fast motion of the electrons, at energies of $O(E_F)$ away from the Fermi level, “dresses” the bare electrons and forms quasi-particles. The Landau Fermi-liquid theory describes this dressing process [14,15] and the way it renormalizes the system parameters. In Appendix B we use this theory to estimate J_s for several situations.

The Fermi-liquid “dressing” continues up to energies of order $1/\tau$. Below $1/\tau$ the motion of the electrons becomes diffusive and new diffusion singularities appear. In a situation where one of the dimensions of the system is much smaller than the others, the system may become quasi-two-dimensional at frequencies smaller than the Thouless energy that is related to the short di-

¹ The symmetry index β counts the degrees of freedom of the matrix elements of the single particle Hamiltonian, $\beta = 1, 2$, or 4 if its elements are real complex or real quaternion numbers, respectively. A magnetic flux $\sim \phi_0/\sqrt{g}$ through the dot, where $\phi_0 = hc/e \approx 4.12 \times 10^{-13} \text{Tesla} \cdot \text{m}^2$, leads to a time reversal symmetry breaking.

mension. This reduction in the dimension of the system enhances the diffusive singularities and changes the flow of the interaction parameters[16]. It appears that the RG flow in the Cooper channel is sensitive to disorder more than the RG flow in the other channels[16], (see also Appendix C). However, in certain situations, especially when disorder is strong, we also have to consider its effect on the flow in the other channels[16].

Finally, we arrive at temperatures $T < E_{\text{Th}}$ and are left with an effective “zero dimensional” Hamiltonian, \mathcal{H}_{eff} . The length scale associated with such low temperatures is larger than the system size and therefore the interaction parameters are constants that do not depend on the site or state index. We note that in ballistic samples, *i.e.*, when the electrons cross the sample before suffering substantial scattering from impurities we may use the Fermi-liquid theory, without additional complications due to the diffusive motion at intermediate scales.

2.1.1 Fluctuations in the interaction parameters

In practice, not all the samples have exactly the same shape and/or impurity configuration, we therefore expect to find sample to sample (mesoscopic) fluctuations in the RG process that will lead to fluctuations in the interaction constants of the different channel. By assumption (that is motivated and supported by numerical analysis [17,18]) the sample to sample fluctuations in the single particle levels are described by random matrix theory. The eigenenergies and eigenfunctions are those of a random matrix.

The random electron states have random charge distributions and hence we expect that the interaction parameters J_c , U_c and J_s themselves will fluctuate with the electron number. The interaction in the Cooper channel is reduced by a logarithmic factor (see Appendix C) and we will neglect its fluctuations.

When an electron is added to the system charge flows to the dot edges and leads to fluctuations in the self-consistent nonuniform potential [19]. These fluctuations scale as $\sim (r_s/\sqrt{g})\Delta$, and give the largest contributions to the fluctuations in U_c . [See Eqs. (B.3) and (B.7) for a precise definition of r_s in two and three dimensions.] Fluctuations in U_c are relevant to the Coulomb peak spacing distribution (Subsection 2.3.1) and to nonequilibrium effects (Subsection 4.2) in the conductance through the dot at finite bias voltage.

The short range part of the Coulomb interaction determines the exchange integral in the expression for the exchange interaction parameter J_s . We can therefore use a contact interaction model to find its fluctuations. The fluctuations in the interaction parameter in that case, for three dimensional samples, are [20] $\sqrt{\text{var } J_s} \approx J_s \max \left\{ 1/(2\sqrt{2N}), c_3/g \right\}$, where c_3 is a numerical number

of order 1, and $N \sim E_F/\Delta$ is the total number of electrons in the dot. The first term is larger for $g^2 \gg N \Leftrightarrow L < (k_F l)l$, with L the sample size, l the mean free path, and k_F the Fermi momentum. For ballistic systems $l \approx L$, and the first term is much larger. Semiclassically [21], the first contribution arises from direct trajectories between two points in the dot, and the second is built from indirect trajectories with possible scattering on the surface or on static impurities. In two dimensional samples a similar calculation [12,13] gives, $\sqrt{\text{var } J_s} \approx J_s \max \{c_2 \log N/\sqrt{N}, c'_2/g\}$, where c_2 and c'_2 are of order 1. For ballistic systems we find that, as in three dimensional samples, the first term is larger.

The actual contribution of the fluctuations in J_s to the fluctuations in the ground state energy is larger by a factor $\sim \sqrt{g}$, as in the calculation of the ground state energy we have to include interaction of a single spin with $\sim g$ electrons [12].

In any case, in the universal limit, when $g, N \rightarrow \infty$ we can neglect the fluctuations in the interaction parameters.

2.1.2 A toy model with contact interaction

In Ref. [3] we discussed a model with contact interaction, described by the Hamiltonian

$$\mathcal{H}_{\text{toy}} = \sum_{n,m,s} c_{n,s}^\dagger \mathcal{H}_0(n,m) c_{m,s} + uM \sum_n c_{n,\uparrow}^\dagger c_{n,\downarrow}^\dagger c_{n,\downarrow} c_{n,\uparrow}. \quad (2)$$

Now m runs over M coarse grain sites (in real space) and $\mathcal{H}_0(n,m)$ is a random matrix. The parameter u describes the strength of the interaction between the electrons.

This toy model was analyzed within the self consistent Hartree–Fock approximation in the limit of large M [3]. We will show in Appendix A that to first order in u the toy model (2) is equivalent to the Hamiltonian (1) with parameters

$$U_c = u/4, \quad J_s = -u \text{ and } J_c = u. \quad (3)$$

Higher order corrections in u preserve the symmetry and the structure of Hamiltonian (1) but give different values for its parameters. In particular, as shown in Appendix C for positive u (which corresponds to a repulsive interaction) they reduce J_c by a factor $\propto \log M$.

2.2 Ground state spin distribution

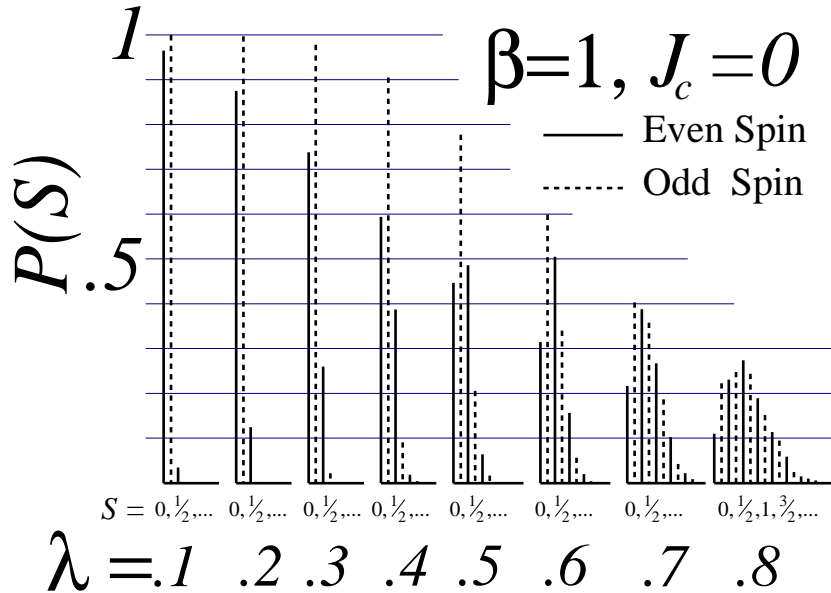


Fig. 1. The probability distribution $P(S)$ of the ground state spin of a quantum dot, computed from Eq. (4) for different values of the interaction parameter $\lambda = -J_s/\Delta$ with time reversal symmetry. Solid histograms are for integer spins, dotted ones for half-integer spins. All the graphs are starting with spin 0 increasing to the right in increments of $1/2$ spin.

In this section we will study the ground state spin of Hamiltonian (1) assuming that the interaction constant $J_c = 0$ [as it renormalized towards zero by electrons with energy larger than the Thouless energy and is further renormalized within the toy model (see Appendix C)]. In this case, the Hamiltonian (1) becomes noninteracting within each spin sector. For a fixed number of particles N we can neglect also the charging energy U_c . The spin of the ground state is then found by minimizing the energy $E_G(S)$ of the lowest lying state with total spin S , as a function of S . Since the lowest energy state with spin S has precisely $2S$ singly occupied states, all lower lying states being doubly occupied, one has [3]

$$E_G(S) - E_G(S_0) = \sum_{\mu=1}^{S-S_0} (\varepsilon_{N+\mu+2S_0} - \varepsilon_{N+1-\mu}) + J_s [S(S+1) - S_0(S_0+1)]. \quad (4)$$

where $S_0 = 0$ ($1/2$) if the total number of particles N is even (odd). Since the precise positions of the energy levels $\{\varepsilon_\mu\}$ in Eq. (4) fluctuate from grain to grain, the ground state spin S does so as well. Plots of the probability distribution $P(S)$ are shown in Fig. 1 and Fig. 2 for different values of the

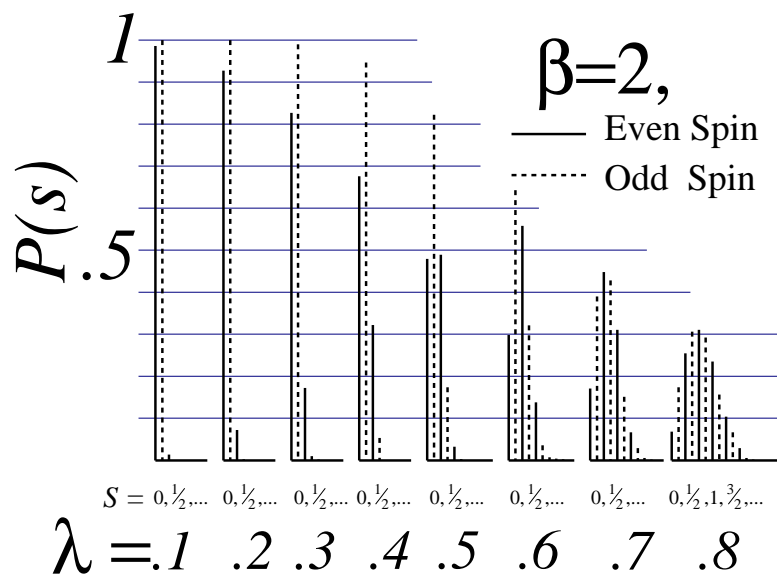


Fig. 2. The probability distribution $P(S)$ of the ground state spin of a quantum dot, computed from Eq. (4) for different values of the interaction parameter λ without time reversal symmetry. Solid histograms are for integer spins, dotted ones for half-integer spins. All the graphs are starting with spin 0 increasing to the right in increments of $1/2$ spin.

dimensionless parameter $\lambda = -J_s/\Delta$. The effective parameter λ , that includes renormalization from fast electrons, is calculated for small metallic dots and semiconductors dots in Appendix B. The distributions are obtained by taking the levels ε_μ from the GOE ($\beta = 1$), or, when time-reversal symmetry is broken, from the GUE, ($\beta = 2$), and minimizing Eq. (4) with respect to S . The way spin-orbit coupling reduces the effect of the interaction in the exchange channel is discussed in Sec. 3.2.

2.3 Application to Coulomb Blockade statistics

A few experimental results on the statistics of the Coulomb blockade peak spacing in a quantum dot [7–9] suggest that the predictions of the constant interaction model, with single-particle levels taken from RMT and with a constant charging interaction U_c only, fails to describe the fluctuations of Coulomb blockade peak spacing. The RMT+ U_c -model predicts a Wigner surmise peak distribution, and even-odd effects. But experimentally, the peak spacing distribution is roughly Gaussian (with non Gaussian tails), its width is $\gtrsim \Delta$ [9], and even-odd effects are not observed. Numerical studies for a few electrons, with mutual Coulomb repulsion, in a disordered medium [17] deviate from the predictions of the RMT+ U_c -model as well.

We will discuss now what the model (1) predicts for the Coulomb blockade peak spacing distribution. By definition, the spacing between the N 'th Coulomb peak and the $N - 1$ 'th Coulomb peak is given by

$$\Delta E = (E_{N+1} - E_N) - (E_N - E_{N-1})$$

where E_N is the energy of the system with N electrons. Fluctuations in the single particle energy levels $\{\varepsilon_\mu\}$, and in the interaction parameters U_c , J_s and J_c may lead to fluctuations in ΔE as N changes. The latter, however, vanish when $g \rightarrow \infty$. As we discussed in the previous section, the fluctuations of the single particle levels induce fluctuations in the ground state spin of the dot even when the interaction constants J_s , U_c and J_c do not fluctuate with N . These, in turn, cause fluctuations in the peak spacing.

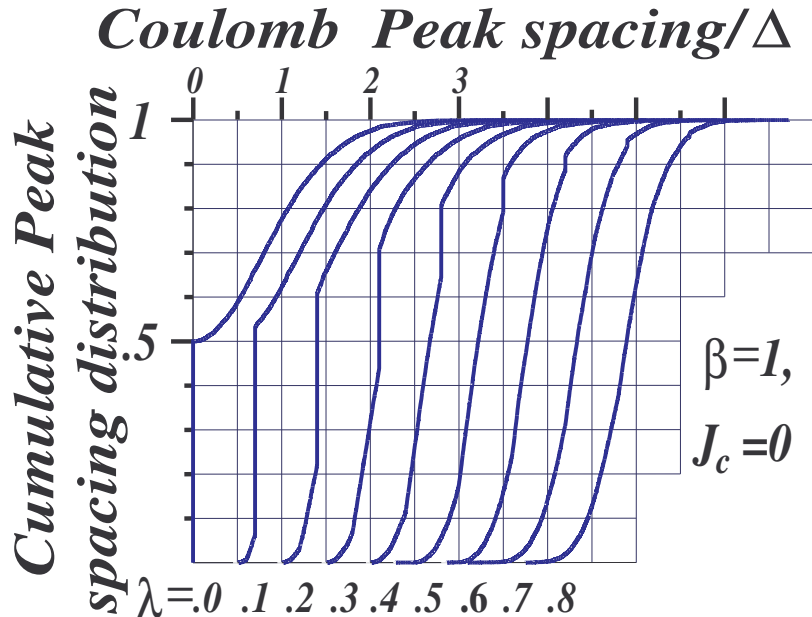


Fig. 3. Theory for cumulative Peak spacing distribution in the presence of time reversal symmetry ($\beta = 1$). We show the case without interaction in the Cooper channel ($J_c = 0$) as it is suppressed (see Appendix C). For clarity we shift the distributions with exchange parameters $\lambda = -J_s/\Delta$ in intervals of half of the average level spacing, Δ .

In Fig. 3 we plot the cumulative Coulomb peak spacing distribution for ensembles with a GOE symmetry. As discussed in Appendix C the interaction in the Cooper channel is suppressed (by a logarithmic factor). We therefore plot in Fig. 3 the cumulative peak spacing distribution for a GOE ensemble without interaction in the Cooper channel ($J_c = 0$). Fig. 3 shows the distributions for exchange interaction strengths of $\lambda = -J_s/\Delta = 0, 0.1, \dots, 0.8$. We choose to plot the *cumulative* peak spacing distributions and not histograms of the peak spacing density distribution. Plotting the cumulative distribution allows us to represent delta functions in the spacing distribution and avoids the need to

work with arbitrarily binning intervals, as is needed for a histogram.

Examining Fig. 3, one notices that there is a jump in the cumulative Coulomb peak spacing distribution at energy $\Delta E = 2\lambda\Delta$, corresponding to a delta function in the spacing distribution at that energy. This occurs because there is a finite probability that starting from a spin-singlet ground state, two successive electrons will enter with opposite spin into the same single-particle state, and the quantity $2\lambda\Delta$ is the exchange energy cost for adding the second electron, when $J_c = 0$. However, at large values of λ the probability that the ground state of the dot is a singlet is smaller, hence the height of the jump decreases. There is an additional substructure of the distributions (*e.g.* a kink in the lower part of the distribution) that becomes smoother when λ increases. To understand a few details of the Coulomb peak spacing distribution curve, we have to find the ground state energies of a disordered system with $N - 1$, N and $N + 1$ electrons. (We assume that the system has the same disorder realization for consecutive electron entries.)

The ground state of a system with N electrons is also characterized by its spin S . Few examples of the energies of states $|N, S\rangle$ are summarized in Fig. 4. The Coulomb peak spacing is given by $\Delta E = E_{N-1, S_{N-1}} + E_{N+1, S_{N+1}} - 2E_{N, S_N}$, where $E_{N, S} = \langle N, S | \mathcal{H}_{\text{eff}} | N, S \rangle$ is the energy of the state $|N, S\rangle$. [Notice that in the presence of interaction in the Cooper channel $|N, S\rangle$ is not necessarily an eigen state of \mathcal{H}_{eff} , defined in Eq. (1)]. Different values of S_{N-1}, S_N, S_{N+1} give rise to different spin sequences.

There are few possibilities for sequences of spin entries, (see Table 1). Sequence #1 describes a situation where initially there are $(2m - 1)$ electrons in the system. The first $2(m - 1)$ single particle states are doubly occupied, and the last state (state m) is singly occupied. We denote this state by $|1, 1/2\rangle$, see Fig. 4. Then an electron is added to state m so that it is doubly occupied, we denote this state by $|2, 0\rangle$. The third electron is added to state $m + 1$ so that it is singly occupied to form the state $|3, 1/2\rangle$. The peak spacing of this sequence is:

$$\begin{aligned} \Delta E_1 &\equiv E_{1, 1/2} + E_{3, 1/2} - 2E_{2, 0} \\ &= U_c + 3/4 J_s + 9U_c + \delta + 3/4 J_s + J_c - 2(4U_c + J_c) \\ &= 2U_c + 3/2 J_s - J_c + \delta = \delta - u - J_c \equiv \Delta T_1. \end{aligned}$$

In the last equality we have used relation (3) for the contact interaction toy model. The peak spacings for other sequences, calculated in a similar way, are summarized in Table 1.

Sequence #1 occurs only if $E_{2, 0} < E_{2, 1} \Leftrightarrow \delta > J_c - 2J_s \Leftrightarrow \Delta T_1 > u$. In a similar way one can check that sequence #2 occurs when $\Delta T_2 > u$. Thus, both processes #1 and #2 will lead to a step in the peak spacing distribution at u . For the cumulative peak spacing distribution, this will lead to a discontinuity

			$ N,S\rangle$	$E_{N,S}$
$m+2$	—	—	$ 0,0\rangle$	0
$m+1$	—	—		
m	—	—		
$m+2$	—	—	$ 1, \frac{1}{2}\rangle$	$U_c + \frac{3}{4}J_s$
$m+1$	—	—		
m		—		
$m+2$	—	—	$ 2,0\rangle$	$4U_c + J_c$
$m+1$	—	—		
m				
$m+2$	—	—	$ 2, 1\rangle$	$4U_c + 2J_s + \delta$
$m+1$		—		
m		—		
$m+2$	—	—	$ 3, \frac{1}{2}\rangle$	$9U_c + \frac{3}{4}J_s + J_c + \delta$
$m+1$		—		
m				
$m+2$	—	—	$ 4, 0\rangle$	$16U_c + 4J_c + 2\delta$
$m+1$		—		
m				
$m+2$	—	—	$ 4, 1\rangle$	$16U_c + 2J_s + J_c + \delta + \tilde{\delta}$
$m+1$		—		
m				

Fig. 4. Possible spin configurations of the dot and their energies according to Eq. (1). We assume that all states below level m are doubly occupied and denote this many body state $|0,0\rangle$. The single particle states are: $\epsilon_m = 0$, $\epsilon_{m+1} = \delta$, $\epsilon_{m+2} = \tilde{\delta}$.

in the slope of the curve, which may be seen in Fig. 3 at the points $\Delta E = \lambda\Delta = -J_s$. Processes #1 and #2 are the main contributions to the approximately linear portions of the curves in the range $-J_s = \lambda\Delta < \Delta E < 2\lambda\Delta = -2J_s$, which are seen at small values of λ .

Sequence #3 will occur if $E_{2,0} < E_{2,1}$ and $E_{4,0} < E_{4,1}$. This occurs if $J_c - 2J_s < \delta < \tilde{\delta}2J_s - 3J_c$ and leads to a step function jump in the cumulative peak distribution at ΔE_3 . This is clearly seen in the theoretical curves of Fig. 3 and Fig. 5. The weight of the jump is bounded from above by $\int_{\Delta E_3}^{\infty} p(\delta')d\delta'$ where $p(\delta')$ is the Wigner distribution for consecutive levels at distance δ' .

Sequence #5 requires that $E_{2,1} < E_{2,0}$ and $E_{4,0} < E_{4,1}$, which occurs when

i	Spin Configurations	ΔE_i	ΔT_i
1	$ 1, 1/2\rangle \Rightarrow 2, 0\rangle \Rightarrow 3, 1/2\rangle$	$2U_c + 3/2 J_s - J_c + \delta$	$-u - J_c + \delta$
2	$ 1, 1/2\rangle \Rightarrow 2, 1\rangle \Rightarrow 3, 1/2\rangle$	$2U_c - 5/2 J_s + J_c - \delta$	$3u + J_c - \delta$
3	$ 2, 0\rangle \Rightarrow 3, 1/2\rangle \Rightarrow 4, 0\rangle$	$2U_c - 3/2 J_s + J_c$	$2u + J_c$
4	$ 2, 0\rangle \Rightarrow 3, 1/2\rangle \Rightarrow 4, 1\rangle$	$2U_c + 1/2 J_s + \tilde{\delta}$	$\tilde{\delta}$
5	$ 2, 1\rangle \Rightarrow 3, 1/2\rangle \Rightarrow 4, 0\rangle$	$2U_c + 1/2 J_s + 2J_c + \delta$	$+ 2J_c + \delta$
6	$ 2, 1\rangle \Rightarrow 3, 1/2\rangle \Rightarrow 4, 1\rangle$	$2U_c + 5/2 J_s - J_c + \tilde{\delta}$	$-2u - J_c + \tilde{\delta}$

Table 1 The symbol ΔE_i denotes the spaces between the Coulomb peaks for spin sequences i . [ΔT_i is ΔE_i using the parameters of the toy model, Eq. (3).] Sequences that involve higher spins are also possible and are not included in this table. To find the actual contribution to the peak spacing we should include the probability that such a sequence occurs.

$\delta < \min\{J_c - 2J_s, \delta - 3J_c + 2J_s\}$. This leads to a low energy tail in the shape of the Wigner distribution curve, that extend all the way down to $\Delta E = 0$, when $J_c = 0$.

Here we have discussed some of the simplest spin-entry sequences, including situations with total spin 0, 1/2, and 1, and we have seen how these sequences appear in the cumulative peak spacing distribution. Generalizations for more complex situations are straightforward but tedious. Different sequences will lead to other singularities and smooth curve-segments in the distribution of peak spacings.

The actual numerical calculations (which includes also sequences with spin larger than 1) do not demand, however, a detailed analysis as above. We performed them in the following manner: we use 24 random levels around the center of the spectrum of a random 100×100 matrix for 1000 realizations. For each realization we find, using formula (4), the configuration of the groundstate and its energy for eight consecutive entries of electrons, this gives us 6 peak spacings for each realization, so that totally we plot a histogram of 6000 peaks.

In Fig. 5 we plot the cumulative peak spacing distribution for magnetic field large enough so that the non interacting levels may be described by the GUE ensemble and the interaction in the Cooper channel is completely suppressed. (We assume that the magnetic field is small enough so we can neglect Zeeman splitting effects.)

2.3.1 Comparison between Theory and Experiments

This section compares our theory for Coulomb blockade peak spacing with the available experimental results. We will see below that the agreement be-

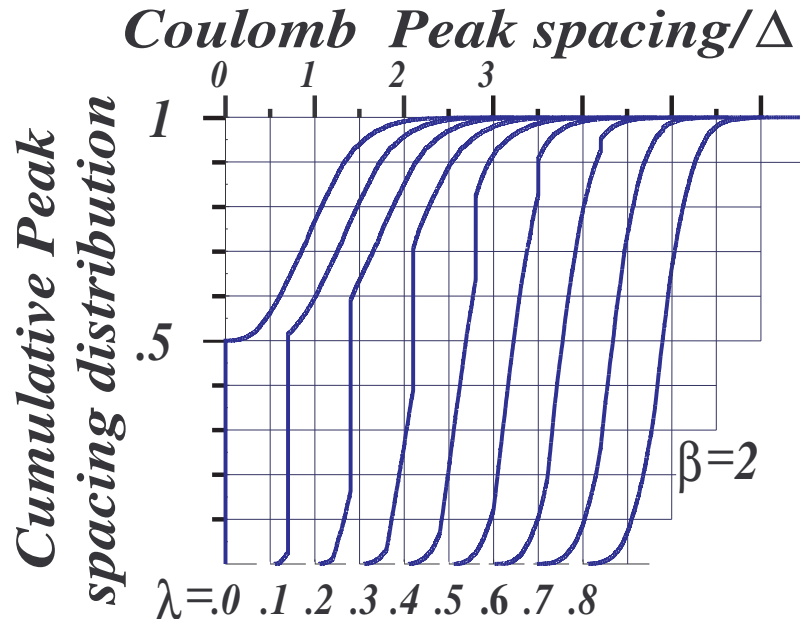


Fig. 5. Theory of cumulative peak spacing distribution in the absence of time reversal symmetry ($\beta = 2$). We assume that the external magnetic field is large enough to break time reversal symmetry, but small enough so that we can neglect Zeeman splitting. In other words, the interaction in the Cooper channel is completely suppressed and the level spacing distribution is described by a GUE ensemble. For clarity we shifted the distributions with exchange parameters $\lambda = -J_s/\Delta$ by intervals of half level spacing.

tween theory and experiment is not very good, particularly for small peak spacings. However some features of the theory are found also in experiments. For example, a non-Gaussian tail at large values of peak spacing and a jump in the cumulative distribution, that we described in the preceding section, are present in few experiments.

Fig. 6 depicts the cumulative peak spacing distribution of AlGaAs-dots. Dots “3-7” were studied in Ref. [9] and dot “S” in [10]. In all the experimental curves that we present here, no magnetic field is applied. We therefore assume in the theoretical analysis that time reversal symmetry is conserved. In each curve we normalize the peak spacing by the dot level spacing, which vary from dot to dot since their sizes are different. We have used here the average level spacings quoted in the experimental papers, there are, of course, some uncertainties in these values. After this normalization we would expect that the curves of dots 3-7 will be similar. This should happen because they have similar electron density and therefore similar r_s and exchange interaction parameter (see Appendix B). In addition we would expect that dot “S” will have a different curve, because it has an electron density that is larger by a factor ~ 3 . However, as Fig 6 shows, the experimental results behave differently. This may be attributed to the intrinsic noise in the system (see Table 1 in [9]), but

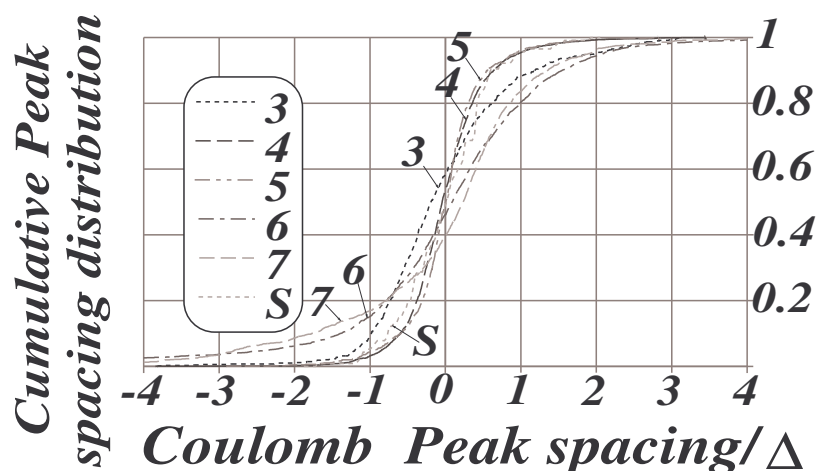


Fig. 6. Experimental results (curves “3-7” [9] and “S” [10]) of the cumulative peak spacing distributions. To compare between the dots of different sizes, we subtract from each distribution the dot average peak spacing and scaled it to the average level spacing, Δ . The dots here have time reversal symmetry.

we still do not understand completely the origin for this behavior. The data of

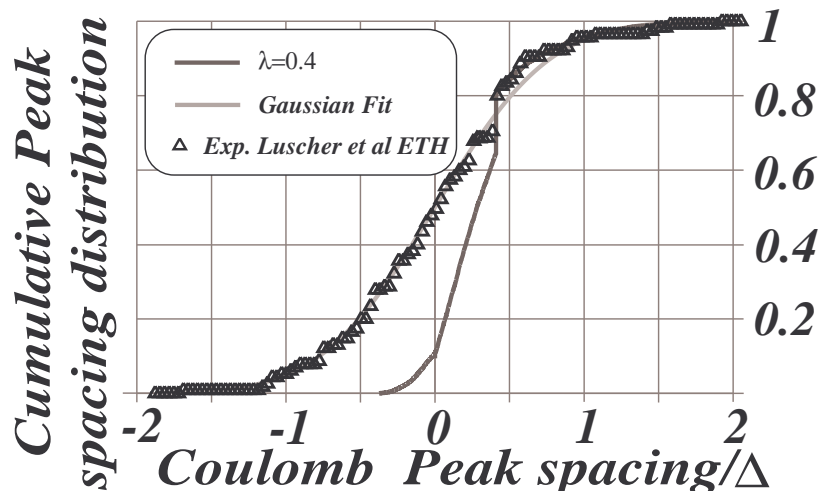


Fig. 7. Comparison between theory and experiment[10]. To fit best the upper tail of the experimental results in the absence of magnetic field, we choose in the theory (with GOE symmetry but without interaction in the Cooper channel) $-J_s/\Delta = \lambda = 0.4$.

Refs. [7] and [8] show a significantly wider distribution of level spacings than found in Ref. [9], despite the apparent similarity of the systems studied by these groups. So far, there has been no clear explanation for this discrepancy.

We nevertheless plot in Fig. 7 our theory and the experimental curve of [10] (without magnetic field). The overall experimental curve fits well to a Gaus-

sian. However, the details of the upper (right) tail of the cumulative distribution, *i.e.*, the jump and the non Gaussian tails fits better to the theory of the spin fluctuations in the Ground state. To fit best the upper tail of the experimental results in the absence of magnetic field, we choose in the theory (with GOE symmetry but without interaction in the Cooper channel) $-J_s/\Delta = \lambda = 0.4$. Notice that using the static RPA estimate of λ (in Appendix B), with the experimental value $r_s \sim 0.72$ [10] we find, as expected, a value that is somewhat smaller than 0.4.

We expect that several effects, (not included in the theory) may be important for current experiments. The lower part of the peak spacing distribution, that is built from single particle levels that are, by chance, very close to each other, is especially sensitive to these effects. Indeed, this part appears to be far from the theoretical curves. Among them are:

- (1) Non universal effects of finite g that cause fluctuations in the interaction parameter [12]. For ballistic two-dimensional dots $g = \sqrt{2\pi nA}$, where A is the dot area and n is the density of the electrons. In the dots of Ref. [7–9] $r_s \sim 1 - 3$ and $g \sim 50 - 150$ (in these of Ref. [10] $r_s \sim 0.72$ and $g \sim 35$). Thus, when we compare theory to experiment, fluctuations in the interaction constants cannot always be ignored. Ullmo and Baranger present in Ref. [12] a detailed study of the effect of fluctuations of the interaction parameters (see also the discussion here in page 6). They find indeed that when these fluctuations are included the results “are significantly more like the experimental results than the simple constant interaction model”.
- (2) We assume that the temperature, and the single particle levels width (due to tunneling to the leads), is smaller than the mean level spacing and therefore we ignore their effects. This assumption is not valid for the lower part of the distribution as it is built from levels whose distance from neighboring levels might be much smaller than the average level spacing. The importance of the temperature was considered very recently by Usaj and Baranger [22]. They find that temperature effects are significant even at $T \sim 0.1\Delta$.
- (3) There is experimental noise due to charge motions during the measurements time. This effect [9] might be the dominant contribution to the smearing of the distribution in the experimental curve.

3 Spin-Orbit Effects

Spin-orbit coupling can have major effects on the ground states or the low-energy transport properties of a mesoscopic system. In many metallic nanoparticles, spin-orbit effects arise from randomly placed heavy-ion impurities, which

can simultaneously scatter electrons and flip their spin, subject to the constraints imposed by the requirement of time-reversal invariance in the absence of an applied magnetic field. In other cases, one is concerned with metal particles where the spin-orbit effects are already significant in the band-structure of the ideal host crystal, so that the “spin” variable in the Bloch states actually represents a mixture of spin and orbital degrees of freedom at the microscopic level. In this case spin-flip scattering with the requisite spin-orbit symmetry can occur whenever there is scattering: from defects, from impurities, or from the boundaries of the sample. Spin-orbit scattering in the above cases can generally be characterized by a spin-orbit scattering rate, and the importance of spin-orbit effects is determined by the ratio of this rate to other frequencies characteristic of the mesoscopic system. Effects of spin-orbit scattering on the groundstate spin-structure and on the energy splitting in an applied magnetic field will be discussed in Subsection 3.1. The effects of spin-orbit coupling on the spacing of groundstate energies, in the presence of electron-electron interactions, will be discussed in Subsection 3.2.

A peculiar situation can arise in two-dimensional electron systems in materials such as GaAs. Here the dominant spin-orbit effects arise from terms in the effective Hamiltonian in which there is a coupling to the electron spin linear in the electron velocity. (These terms arise from the asymmetry of the potential well confining the electrons to two dimensions and from the lack of inversion symmetry in the GaAs crystal structure.) The special form of this coupling leads to a large suppression of spin-orbit effects when the 2D electron system is confined in a small quantum dot. However, effects of spin-orbit coupling are again enhanced in the presence of a strong magnetic field parallel to the plane of the sample, so that they must be taken into account in such properties as the level-spacings of a closed dot or the statistics of conductance fluctuations in a dot coupled to leads through one or more open channels. These effects will be discussed in Subsection 3.3 below.

3.1 Effective g -tensor of a metal particle with spin-orbit scattering.

According to Kramers theorem, a metal particle with an odd number of electrons with no special symmetry, in zero magnetic field, must have a degenerate groundstate manifold, with pairs of states related to each other by time-reversal symmetry. In the absence of spin-orbit coupling, the total spin S is a good quantum number, and the groundstate manifold is just that expected for half-integer S . As we have seen in Sec. 2, if the electron-electron interaction is weak, we will essentially always find $S = 1/2$ for odd N and the ground state will be just two-fold degenerate. For stronger electron-electron interactions, however, there will be some probability of finding $S = 3/2$ or larger, so that four-fold or higher degeneracies are also possible. When spin-orbit interactions

are turned on, the higher degeneracies will be broken into a set of doublets, so that the ground state will again be two-fold degenerate.

If we now apply a magnetic field B to the system, the degenerate ground state will be split. For sufficiently small B , one of the states will move up in energy by an amount $\delta\varepsilon$ which is linear in B , while the other state will move down by the same amount. These shifts may be measured, at least in principle, by electron-tunneling spectroscopy experiments in an applied magnetic field. We discuss here the statistical properties of the distribution of energy shifts expected under various circumstances. We concentrate on the situation where the electron-electron interaction is weak, so that the many-body ground state is well described by the picture of weakly interacting quasiparticles, as effects of electron-electron interactions will be discussed in the next subsection.

Quite generally, we may write the linear splitting of a Kramers doublet in the form

$$\delta\varepsilon = |\mu_B/2|(\vec{B} \cdot \overleftrightarrow{K} \cdot \vec{B})^{1/2} \quad (5)$$

where $\mu_B < 0$ is the electron Bohr magneton and \overleftrightarrow{K} is a real, positive-definite symmetric 3×3 tensor. In the absence of spin-orbit coupling, \overleftrightarrow{K} is isotropic, with $K_{ij} = 4\delta_{ij}$. When spin-orbit coupling is present, we find that \overleftrightarrow{K} varies from level to level, and is in general anisotropic. We write the three eigenvalues of \overleftrightarrow{K} as g_k^2 , ($k = 1, 2, 3$), with $|g_1| \leq |g_2| \leq |g_3|$, and refer to the g_k 's as the three principal g -factors for the level. Although the energy-splittings in a static magnetic field only define the absolute values of the g_k , by considering the response to a time-varying magnetic field (e.g., a spin resonance experiment) one can also give an unambiguous meaning to the sign of the product of the three g -factors. Since the sign of an individual g_k has no physical meaning, we adopt the convention that g_3 and g_2 are always positive, but g_1 can be positive or negative, depending on the specific system considered.

For the case of weakly interacting electrons, which we consider here, the ground state for $2N + 1$ electrons consists of $2N$ electrons in filled Kramers doublets, plus one electron in a doublet which is singly occupied. The filled doublets give no contribution to the linear energy shift because in each case one state moves up and the other moves down by the same amount. Thus, the g -factors are determined by the properties of the singly-occupied state.

In the presence of spin-orbit coupling there are two contributions which can shift the g -values from the bare value $g = 2$. If we take into account only the interaction of B with the electron spin, then spin-orbit coupling will always reduce the g -values. For example, if the magnetic field is applied in the z -direction, the state which is shifted down in energy will be the particular linear combination of the two degenerate states which has the maximum expectation

value of $-S_z$. This expectation value is $\leq 1/2$, so the spin-contribution to the g -factor will generically be reduced by spin-orbit coupling.

On the other hand, there is also an orbital contribution to the linear Zeeman effect, when spin-orbit coupling is present. (In the absence of spin-orbit coupling, the orbital states in an irregular dot will be generically non-degenerate and time-reversal-invariant, so they cannot acquire a linear energy shift in a weak magnetic field.) Both the orbital and spin contributions were considered by Matveev *et al.* [23], who discuss the expectation value and probability distribution of $\delta\varepsilon^2$ for the magnetic field in an arbitrary fixed direction.

By contrast Brouwer *et al.* [24] considered the joint probability distribution of the three g -values for a single level, so they could examine the anisotropy as well as the magnitude of the g -tensor. Their analysis concentrated on the case where orbital effects can be ignored, so that the mean-square g -factors are monotonically reduced with increasing spin-orbit coupling. The strength of the spin-orbit coupling in this case is determined by a parameter

$$\lambda_{\text{so}} = \sqrt{\frac{\pi\hbar}{\tau_{\text{so}}\Delta}} \quad (6)$$

where Δ is the mean separation between one-electron energy levels. The mean spin-orbit scattering time τ_{so} is defined so that if we prepare a state with spin up, the probability to find it in the same spin direction after time t is $\sim e^{-t/\tau_{\text{so}}}$. When $\lambda_{\text{so}} \gg 1$, one finds that the g -factors are greatly reduced from their bare values, and one can obtain an analytic form for the joint probability distribution:

$$P(g_1, g_2, g_3) \propto \prod_{i < j} |g_i^2 - g_j^2| \prod_i e^{-3g_i^2/2\langle g^2 \rangle} \quad (7)$$

For intermediate values of the coupling parameter λ_{so} , one can perform numerical simulations to study the distribution, using random-matrix theory. In Fig. 8 we show the λ_{so} -dependence of the mean values of g_k^2 , as well as the values of g_k for a particular realization of the random matrices.

Very recently, Petta and Ralph [Ref. [25]] have measured effective g -values for a number of levels in each of several different nanoparticles, of Cu, Ag and Au, with diameters in the range 3 - 5nm. They did not vary the direction of the applied magnetic field, so they could not study the anisotropy of the g -tensor. However, the statistical distributions of the g -factors (normalized to their means) for different levels in a given particle were found to be in good agreement with the theories of Refs. [23] and [24]. For the mean g -factor, an agreement with Refs. [23] and [24] is found if the spin contribution is taken into account only; the mean g -values observed in the Au particles (ranging from

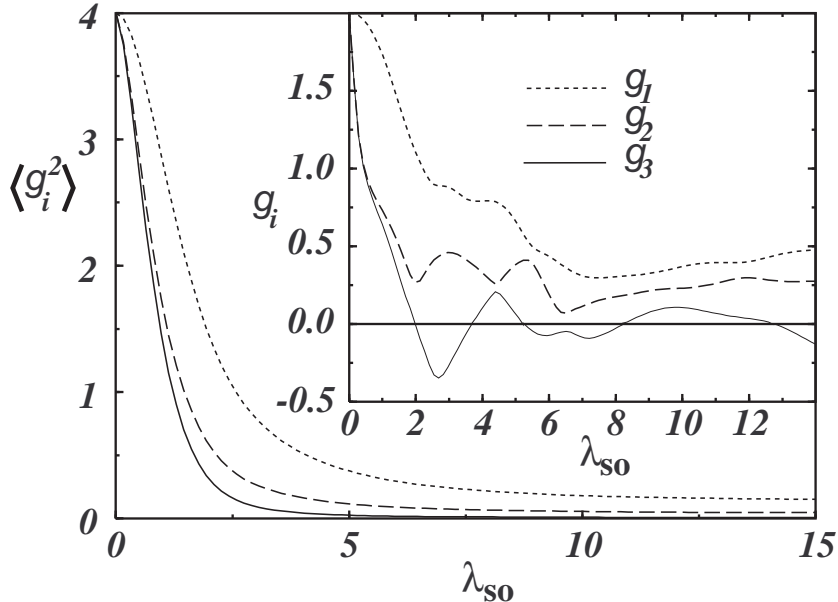


Fig. 8. Average of the squares of principal g -factors versus spin-orbit scattering strength λ_{so} , obtained from numerical simulation of a random matrix model. Inset: g_1 , g_2 , and g_3 for a specific realization. We have included the sign of g_1 .

0.12 to 0.45) were significantly smaller than what one might expect from the orbital contribution, according to the theory of Ref. [23], unless one assumes a very short mean-free-path for the electrons. (Using the formulas in Ref.[23], one would need a mean-free-path of order $0.1nm$ to get g -values this small.) Small g -values (below 0.5) for Au nanoparticles were also observed previously by Davidovic and Tinkham [4].

3.2 *Effects of spin-orbit coupling on interaction-corrections to groundstate configurations and energy spacings.*

So far, we have ignored the effects of electron-electron interactions. This should generally be valid if the exchange interaction is small compared to the threshold for the Stoner instability, so that the probability of finding $S > 1/2$ is small in the absence of spin-orbit coupling. When the spin-orbit coupling parameter λ_{so} is large, the effective exchange interaction between two electrons in states close to the Fermi-energy of the particle will be even further reduced, as the mean spin in any state becomes small compared to $1/2$, and the local spin orientations have different spatial distributions for one-electron states belonging to different Kramers doublets.

In the limit of very large spin-orbit coupling, where the mean spin tends to zero, the exchange interaction should also tend to zero. This means that the

parameter J_s in the effective Hamiltonian (1) of Sec. 2.1 should be set to zero. This is consistent with the fact that spin is no longer a good quantum number of the system, and the term proportional to J_s is no longer invariant under the set of allowed unitary transformations of the random matrices.

A consequence of this analysis is that if a spin-orbit scatterers are added to a system with fixed electron-electron interaction (fixed r_s) the probability distribution for the separation of successive groundstate energies, measured by the Coulomb-blockade peak separations, should approach that of a non-interacting electron system in the symplectic ensemble. This means that there should be a bimodal distribution with an even-odd alternation. The chemical potential to add a second electron to a Kramers doublet is the same as the energy to add the first electron, after the coulomb blockade energy [U_c in Eq. (1)] is subtracted, whereas the chemical potential for the next electron will be larger by an amount approximately given by the mean level spacing Δ .

3.3 Spin-orbit effects in a GaAs quantum dot in a parallel magnetic field.

The most important spin-orbit terms in the effective Hamiltonian for a 2D electron gas (2DEG) in a GaAs heterostructure or quantum well may be written in the form

$$\mathcal{H}_{\text{so}} = \gamma_1 v_x \sigma_y - \gamma_2 v_y \sigma_x \quad (8)$$

where \vec{v} is the electron velocity operator. We have assumed that the 2DEG is grown on a [001] GaAs plane, and we have chosen the x and y axes to lie in the [110] and $[\bar{1}\bar{1}0]$ directions. For an open 2DEG this leads to a spin-orbit scattering rate of order $\gamma^2 D$, where D is the diffusion constant and γ is the geometric mean of the two coupling constants in Eq. (8). For a confined dot of radius R , in zero magnetic field, however, the effects of spin-orbit coupling are suppressed if the typical angle of spin precession for an electron crossing the dot, given by $\theta = \gamma R$, is small compared to unity. One finds in this case that the matrix elements of \mathcal{H}_{so} are greatly reduced for energy states whose energy separation is small.

Halperin *et al.* [26] have argued that the effects of spin-orbit coupling can be enhanced, however, in the presence of an applied magnetic field in the plane. The enhancement is maximum when the Zeeman energy becomes comparable to the Thouless energy (*i.e.*, the inverse of the transit time for an electron in the dot), in which case there is an effective spin-mixing rate comparable to the spin-orbit scattering rate for an open system with an electron mean free-path equal to the mean free path in the dot. For a closed dot, the spin-mixing would be manifest in the repulsion of energy levels for different spin, and the

appearance of anti-crossings of the levels as when the Zeeman field is varied.

Motivated by experiments of Folk *et al.* [27], Halperin *et al.* [26] considered the “universal conductance fluctuations” of a dot connected to a pair of leads with one or more channels open in each lead. They considered explicitly the case where there is a weak magnetic field perpendicular to the dot, so that time reversal symmetry is broken, and the system is in the class of the unitary ensemble, even in the absence of spin-orbit coupling. It was shown that effects of spin-orbit coupling in large Zeeman field could then lead to a factor of two reduction in the variance in the conductance, which is in addition to the factor of two reduction caused by breaking of the spin degeneracy. Calculations of the cross-over, as a function of the in-plane magnetic field, were in at least qualitative agreement with the experimental observations.

Very recently, Aleiner and Fal’ko[28] have considered the case without a perpendicular magnetic field, so that the system without spin-orbit coupling would be in the orthogonal ensemble. They have shown that the application of a parallel magnetic field in this case turns on a spin-orbit perturbation with a special symmetry, so that the system retains an effective time-reversal symmetry even in the presence of the large Zeeman field. The spin-orbit coupling leads to a reduction in the size of conductance fluctuations, but not as much as one would obtain if the time-reversal symmetry was also broken. The spin-orbit coupling also leads to a reduction in the “weak localization” correction to the average conductance, but does not lead to complete suppression as one would find for a broken time reversal symmetry. (However, as noted by Meyer *et al.* [29] and by Fal’ko and Jungwirth[30], for an asymmetric quantum well of finite thickness, application of a strong magnetic field parallel to the sample can lead to broken time-reversal symmetry due to orbital effects, even in the absence of spin-orbit coupling.)

4 Origin of multiplets in the differential conductance

In a recent experiment Davidovic and Tinkham[4] studied tunneling into individual Au nanoparticles of estimated diameters $25nm$, at dilution refrigerator temperatures. The differential conductance dI/dV , as a function of the source-drain voltage V , indicate resonant tunneling via discrete energy levels of the particle. Unlike previously studied normal metal particles of Au and Al, in these samples they find that the *lowest* energy tunneling resonances are split into clusters of 2-10 sub-resonances. The distance between resonances within one cluster is much smaller than the mean level spacing of the Au grain.

This situation is illustrated schematically in Fig. 9. The differential conductance dI/dV shows resonances, where each resonance in dI/dV is actually

a multiplet, the splitting between the peaks of the multiplets being a factor ~ 30 smaller than distance between the resonances (which is of the order single-particle level spacing in the grain).

In this section we outline two-different mechanisms which can lead to a fine structure of the first conductance peak. We first show how such a fine structure can occur if the ground state has a finite spin with small energy splittings between states of different magnetic quantum number. In this model it is necessary to have a relatively large total spin in order to split the conductance peak into many sub-peaks. This mechanism would also be suppressed by large spin-orbit coupling.

In the second mechanism, following Agam *et al.* [31], we show how such a fine structure can arise from nonequilibrium processes induced by the large bias voltage V used in the experiment. This mechanism seems to us to be the more likely one for explaining the observations of Ref. [4]. We also indicate how, experimentally, one might distinguish between the two proposed explanations.

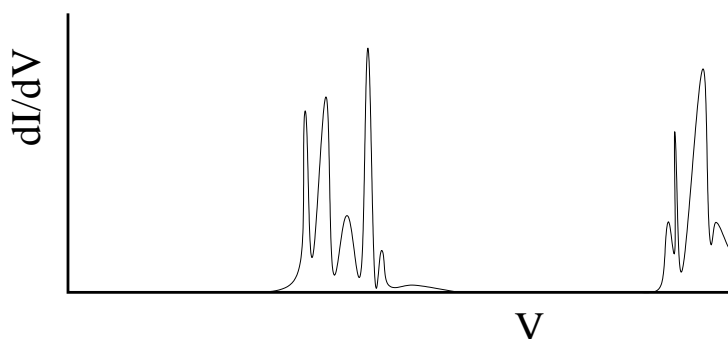


Fig. 9. Schematic illustration of the experimental results of Ref. [4]: The peaks in the differential conductance are split. The distance between the multiplets is of the order of the single particle level spacing Δ ; the distance between peaks in the same multiplet is much smaller.

4.1 Multiplets from an almost degenerate groundstate

In general, a peak in the differential conductance as a function of the bias voltage V may occur if an additional channel for tunneling onto or from the metal grain is opened at that V . The relation between V at the peaks and the ground state energies is complicated; it depends on the capacitive division between the left and right contact and on the conductances of the two tunneling contacts. A detailed account of the possible scenarios can be found in the review by von Delft and Ralph [32].

Here, we make the simplifying assumption that the left point contact has

the bigger resistance and the smaller capacitance, so that the electrostatic potential of the dot equals that of the right reservoir, and the contact to the left reservoir can be seen as the “bottleneck” for current flow. Then, if the grain has N electrons at zero bias, a conductance peak occurs when

$$eV = E_{N+1} - E_N,$$

i.e., when the bias voltage V is precisely equal to the difference of the energies of any two many-body states of the grain with N and $N + 1$ electrons (for $V > 0$), provided the initial N -particle state is populated at the corresponding bias. Below we focus on the first peak in the differential conductance and discuss when and how a fine structure of that first peak can arise. We assume that the temperature is small compared to any splittings in the energy levels, and we assume (for the moment) that there is no spin-orbit coupling.

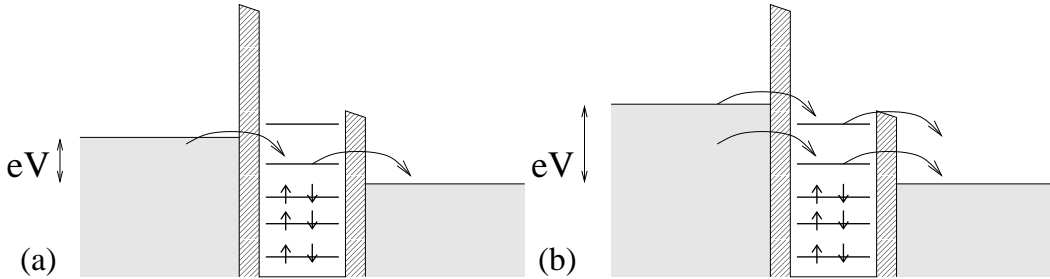


Fig. 10. Schematic drawing of the tunneling process considered here. The left point contact has the smaller capacitance and the smaller conductance. When the bias voltage is increased, peaks in the differential conductance occur, whenever a new channel for tunneling onto or from the grain is opened. Compare the bias voltages in (a) and (b).

If the N and $N + 1$ -particle ground states have perfect degeneracies, the difference $E_N - E_{N+1}$ can only take a single value, and a single peak will be observed, no matter what the spin of the ground state is. Hence to observe a fine structure, the degeneracy of the ground state has to be lifted. This can be done by application of a uniform magnetic field, as is illustrated in Fig. 11 for $S_N = 0$ or $S_N = 1$ and $S_{N+1} = 1/2$. In the case where $S_{N+1} = S_N + 1/2$, the difference $E_{N+1} - E_N$ between the energies of the many-body states for N and $N + 1$ particles can take two values,

$$E_{N+1} - E_N = E_{N+1}^0 - E_N^0 \pm (1/2)g\mu_B B,$$

where E_N^0 and E_{N+1}^0 are the N and $(N + 1)$ -particle energies in the absence of the magnetic field. The differential conductance shows a double peak at voltages

$$eV_{\pm} = E_{N+1}^0 - E_N^0 \pm (1/2)g\mu_B B,$$

as is seen in Fig. 11a. On the other hand, only a single peak at bias voltage $V_+ = E_{N+1} - E_N + (1/2)g\mu_B B$ is found if $S_{N+1} = S_N - 1/2$. Although the bias voltage V_- corresponds as well to a transition energy between many-body

states with N and $N + 1$ particles for $S_N > S_{N+1}$, no peak in the differential conductance is found at that bias voltage, because the initial state of that transition is an excited state, which is not populated at $V = V_-$. Population of an excited N -particle state is only possible at higher bias voltages $V \geq V_+$ via inelastic processes that use the $N + 1$ -particle state as an intermediate step. (A small nonequilibrium population of the excited N -particle state, and hence a small peak at $V = V_-$, may, however, occur as a result of inelastic cotunneling, as is explained in Ref. [33].) If the difference in the total spin quantum numbers for N and $N + 1$ is greater than $1/2$, then there can be no conduction peak at all in the absence of spin-orbit coupling or inelastic cotunneling processes.

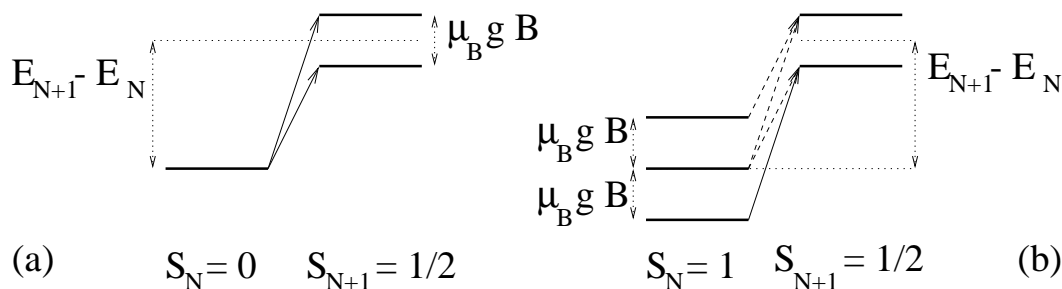


Fig. 11. Possible transitions between Zeeman split states with N and $N+1$ particles, for $S_N = 0$, $S_{N+1} = 1/2$ (a), and $S_N = 1$ and $S_{N+1} = 1/2$ (b). Note that the transitions starting out of the excited states of the triplet in (b), denoted by the dashed arrows, do not give rise to peaks in the differential conductance, (assuming that equilibrium is reached between successive tunneling events), because the excited states are not populated at $eV = E_{N+1} - E_N - \mu_B g B/2$.

The situation changes in the presence of weak static magnetic impurities. “Weak” here means that they can be seen as a small perturbation on top of the picture sketched in the previous sections. “Static” means that the impurity ion has a large intrinsic angular-momentum and large crystal-anisotropy, so that we can neglect the matrix elements for transitions between different impurity spin-states. The impurity spins could be in the grain itself or could be located close to the grain in the surrounding insulator. Then if the many-body state of the grain has non-zero spin, the spin degeneracy will be lifted by the coupling to the impurity spin, which can give rise to a splitting of the lowest conductance peak even in the absence of an applied magnetic field. A significant difference between this case and the splitting due to an external field is that the effective coupling now depends on the microscopic details of the electron wavefunctions close to the impurity, and the level splitting will generally be different for the N and $N + 1$ electron states. As we shall see, this makes it possible for the lowest conductance resonance to split into more than two sub-peaks.

We first consider the case of a single impurity spin. According to the Wigner-Eckart theorem, if the coupling to the impurity spin is weak, an electronic

many-body state with total spin S will be split into $(2S + 1)$ equally-spaced levels, characterized by the quantum number of the magnetic moment in the direction parallel to that of the frozen impurity spin. The size of the splitting depends on the concentration and microscopic details of the impurities. Since a peak in dI/dV can occur whenever $eV = E_{N+1} - E_N$, many close peaks appear when the degeneracy of the ground state is lifted. The total number of possible transitions is $(2S_N + 1)(2S_{N+1} + 1)$, since now E_N and E_{N+1} can take $2S_N + 1$ and $2S_{N+1} + 1$ values, respectively. However, for the same reasons as discussed above, not all possible transitions give rise to peaks in the differential conductance: Only transitions at energy differences $\Delta E = E_{N+1} - E_N$ where the initial N -particle state is already populated at a bias voltage $eV \leq \Delta E$ are reflected as peaks in the differential conductance, and the spin component parallel to the frozen impurity spin can only change by $\pm 1/2$. Some examples are shown in Fig. 12 for $S_N = 1/2$, $S_{N+1} = 1$ and $S_N = 1$, $S_{N+1} = 1/2$. In the figure, the transitions that correspond to true peaks in dI/dV are shown as solid arrows, the other ones are shown with dashed arrows. In practice, since eV is typically much bigger than the fine structure of the N and $N + 1$ -particle levels, all transitions appearing at energy differences ΔE bigger than the difference $eV_{\text{th}} = E_{N+1}^g - E_N^g$ between the ground state energies for N and $N + 1$ particles will show up as true peaks at $eV = \Delta E$, while no peaks appear for $eV < eV_{\text{th}}$ (V_{th} is the threshold voltage for current flow).

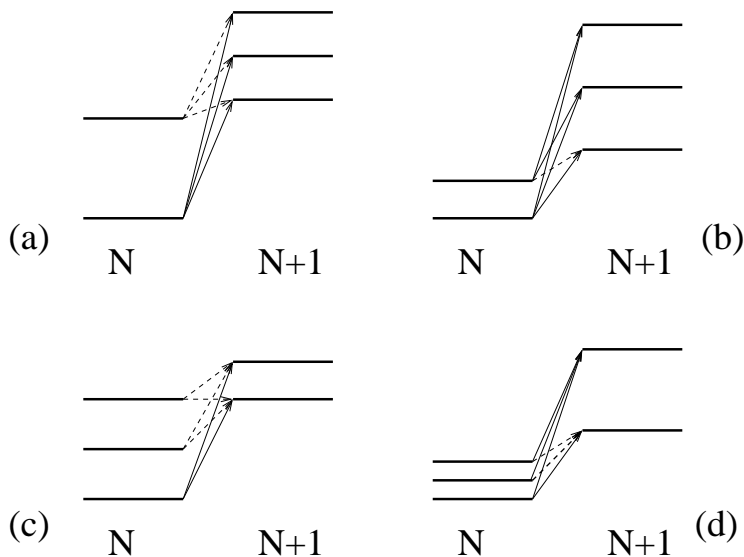


Fig. 12. Possible transitions between states with $S_N = 1/2$, $S_{N+1} = 1$ (top) and $S_N = 1$, $S_{N+1} = 1/2$ (bottom), when the spin degeneracy is broken by the presence of (several) static magnetic impurities. The transitions indicated by solid arrows give rise to peaks in the differential conductance; the transitions indicated by dashed arrows do not, because the state they are starting from is not populated at the corresponding bias voltage. How many peaks are visible depends on the actual splitting of the energies.

If there are several frozen impurity spins coupling to the electrons, we can again use the Wigner-Eckart theorem, in the case of weak coupling, to show that a groundstate with spin S is split into $(2S + 1)$ equally spaced levels classified by the spin component along some direction which is a weighted vector sum of the several frozen impurity spins. The weights in this sum will be different in the states with N particles and with $N + 1$ particles, so that the quantization axes will generally be different in the two states, as well as the level splittings. This will lift the selection rule that the quantum number can only change by $\pm 1/2$ on the addition of a single electron, so the number of lines in the multiplet may increase accordingly.

The model of coupling to one or more frozen spins can also be generalized to the case of dynamical spins. For example, in the case of coupling to a single dynamical localized spin S_i in the insulating material close to the grain, the localized spin and the spin of the electrons in the metal grain S together will form states with total angular momentum ranging from $|S - S_i|$ to $|S + S_i|$, and will split up in the corresponding multiplet. In this case the number of possible transitions depends on the detailed selection rules governing transitions of the localized spin.

Finally, we consider the situation where spin-orbit coupling is present. In the case of weak spin-orbit coupling, a groundstate with spin greater than $1/2$ can be split into several different energy levels even in the absence of an applied magnetic field and in the absence of magnetic impurities (although the splitting by spin-orbit coupling only arises in second order perturbation theory, whereas the splitting caused by magnetic impurities already appears in first order perturbation theory). In general, the various states will be split by different amounts, and so multiple subpeaks can be observed, for large S , just as we found for the case with a frozen magnetic impurity. In the present case, however, states with odd N remain twofold degenerate by Kramers' degeneracy, which reduces the number of possible transitions roughly by a factor of two, compared to the case of static magnetic impurities.

If the spin-orbit coupling is too strong, however, spin-orbit splittings will become comparable to or larger than the single-particle level spacings. In this case, it is no longer possible for splittings between spin states to give rise to fine structure of the conductance peak on a scale small compared to Δ . (Also, as we have seen previously in Subsection 3.2, exchange-splittings tend to be reduced in this case, so that the one electron picture should be valid for the ground states.) The gold particles studied in Ref. [4] appear to be in the strong spin-orbit coupling regime.

4.2 Multiplets from nonequilibrium processes

A second mechanism to observe multiple peak structures in the differential conductance is via nonequilibrium population of highly excited states of the metal grain, as was first proposed by Agam *et al.* [31]. This mechanism does not need a degeneracy, or near-degeneracy, of the ground state. The idea of Ref. [31] is as follows: Since the bias voltage is typically much larger than the spacing Δ between single particle levels, after an electron has tunnelled on and off the grain, the grain may be left in an excited N -particle state, with an occupation of the single-particle levels that differs from the ground state, see Fig. 13. The fact that there is a different occupation of the single-particle levels will slightly shift the addition energies $E_{N+1} - E_N$, thus giving rise to peaks in dI/dV at different values of the bias voltage V . In Ref. [31] spinless particles were considered. In that case, nonequilibrium processes cause a fine structure of the second and higher resonances, but not the first one [31]. For spin $1/2$ particles and even N , the scenario of Ref. [31] can also lead to a fine structure for the first resonance, as we will now describe.

We denote the highest occupied (self-consistent) single-particle level in the N -particle ground state by $\varepsilon_{N/2}$ and assume that the N -particle ground state has zero total spin. When the bias voltage exceeds the threshold $eV_{\text{th}} = E_{N+1}^g - E_N^g$, current flow can leave the grain in an excited N -electron state, when, after an electron has tunnelled into the level $\varepsilon_{N/2+1}$, another electron tunnels out of a lower-lying level ε_ν , see Fig. 13. Note that the excited state can have a total spin $S = 0$ or $S = 1$. Since the grain is now in an N -particle state that is different from the ground state (compare Figs. 13a and c), the energy cost $E_{N+1} - E_N$ for addition of an electron, and hence the position of a peak in dI/dV , is, in general, different from $E_{N+1}^g - E_N^g$. *A priori*, this difference can have three contributions: (1) An electron can tunnel into different single-particle levels than in the ground state. (2) The transition energy $E_{N+1} - E_N$ depends on the spin S of the states involved, which can be different from the ground state spin. (3) All transition energies depend uniquely (but weakly) on the populations of the initial and final states through mesoscopic fluctuations of the interaction contribution to the energy [31]. The characteristic energy scales for the first two of these contributions are Δ and J_s , while the third is of order Δ/\sqrt{g} , as we shall see below, where $g = 2\pi E_{\text{Th}}/\Delta$ is the dimensionless conductance of the grain. For an even N , however, there exist excited N -particle states for which the level $\varepsilon_{N/2+1}$ is only singly occupied and $S = 0$, so that the first two contributions vanish. Then only the contribution from mesoscopic fluctuations remains. If g is large, the energy scale for the fluctuations is small, and one finds multiple conductance peaks close to $eV = E_{N+1}^g - E_N^g$, where the total width of the multiplet is of order Δ/\sqrt{g} .

Although all nonequilibrium configurations have their own characteristic tran-

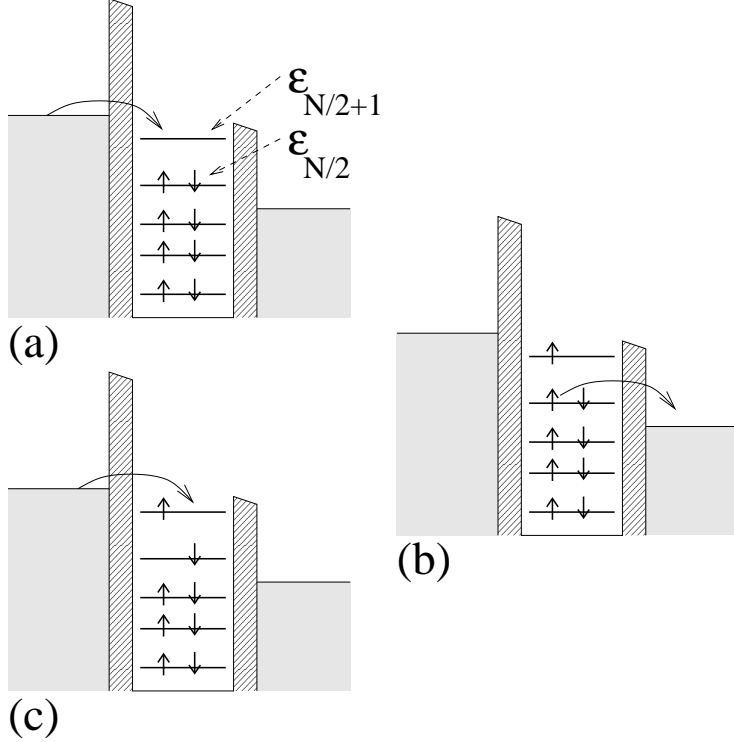


Fig. 13. A nonequilibrium configuration can be obtained from the ground state (a) if an electron tunnels into the first empty level (b), and another electron tunnels off the grain from a different, lower lying, level (c). The energy required for tunneling an electron into the highest level in the configurations (a) and (c) may be different, which explains that more than one peak can be seen in the differential conductance.

sition energy $E_{N+1} - E_N$, not all of them need to correspond to a peak in the conductance; no peak is observed if the corresponding voltage is below the threshold V_{th} , which was needed to populate the corresponding excited state. We estimate that the number of sub-peaks in the first peak multiplet, $N_{\text{first-peak}}$ due to the nonequilibrium effect is of order $eV/2\Delta$, which is roughly the ratio of the Coulomb blockade energy to the single-particle level spacing.

To understand the reasons for this estimate let us first consider the case where we can neglect the exchange coupling J_s in the effective Hamiltonian (1). (This is correct in the case where spin-orbit coupling is strong). We also neglect the Cooper-channel interaction J_c , for the reasons discussed in Appendix C. However, we take into account fluctuations in the size of U_c between different pairs of levels. In this case, the many-body states can be labelled by the occupancies of the single-particle levels, and the ground states with energy E_N^g and energy E_{N+1}^g are described by Fig. 13a and b respectively. Let us assume that V is close to, but slightly above, the threshold voltage $V_{\text{th}} = E_{N+1}^g - E_N^g$. We further assume that when an electron enters or leaves the system it does not excite other electrons by multi-electron processes; in particular we ignore Auger-like processes. Similarly we assume that the only important

contributions to the conductance are via real, energy conserving, transitions.

Under these assumptions, one finds that the excited states that contribute to $N_{\text{first-peak}}$ have precisely one hole below $\varepsilon_{N/2}$. The energy distance between these single-hole states is roughly Δ . Since only excited states within an energy eV from the ground state can be populated, the number of possible hole states is $\sim eV/\Delta$. Of these, roughly half will lead to positive energy shifts, which are necessary for contributions to the multiplet structure, so we find $N_{\text{first-peak}} \sim eV/2\Delta$. The width of the peak is proportional to the size of the fluctuations in U_c that we have discussed in Subsection 2.1.1; in case of long range Coulomb interaction it is $\sim \Delta/\sqrt{g}$.

Many-body states with two or more holes below $\varepsilon_{N/2}$ cannot contribute to the conductance for voltages close to V_{th} , because if two holes are present when there are N electrons on the particle, the level $\varepsilon_{N/2+1}$ will necessarily be doubly occupied. Then, the next electron would have to enter through the level $\varepsilon_{N/2+2}$, which would require an additional energy, of order Δ , that is not available for V slightly above V_{th} . If, by chance, the distance of level $\varepsilon_{N/2+2}$ from level $\varepsilon_{N/2+1}$ is smaller than J_s then transition through nonequilibrium states with two holes may occur. This situation will increase $N_{\text{first-peak}}$ significantly, it should be proportional now to $\sim (U/\Delta)^2/2$.

Let us now consider the case where the exchange parameter J_s is not negligible. Then, the N electron states having one electron in the level $\varepsilon_{N/2+1}$ and one hole below the Fermi energy will have different energies depending on whether they have $S = 0$ or $S = 1$. For $S = 1$, the energy is reduced by $|J_s|$, so that the energy to add the next electron to the level $\varepsilon_{N/2+1}$ is increased by $|J_s|$, and the peaks arising from the triplet configuration will be shifted up by this amount relative to the singlet contributions. If this shift is comparable to the level spacing Δ , then only the singlet peaks will appear close to the threshold, and the number of peaks in the lowest multiplet will be the same as before, $N_{\text{first-peak}} \sim eV/2\Delta$. If $|J_s|$ is sufficiently small, but not negligible, however, the singlet and triplet peaks may appear to form a single multiplet, with twice as many peaks as before.

4.3 A comparison between the mechanisms of Subsections 4.1 and 4.2

The main difference between the two explanations offered here is that the former entails many different transitions between states very close to the N and $N + 1$ -particle ground states, whereas the latter makes use of, in principle, the same transition between different pairs of states that are highly excited above the ground state. Thus, one may distinguish between the two scenarios, when the electrostatic potential of the grain can be changed by the voltage

V_g on a nearby gate: Fine tuning of V_g affects the threshold bias voltage V_{th} , and hence the number of possible nonequilibrium configurations. Hence, if the fine structure of the first resonance is due to nonequilibrium processes, the peaks will disappear one by one when V_g is tuned to the charge degeneracy point. This is illustrated in Fig. 14. In this figure, we have simulated the differential conductance from the rate equations of Ref. [5,34], for the case where all relaxation of excited states inside the grain occurs due to the coupling to the leads. The four panels show the differential conductance for four different values of the gate voltage, where the multiplet consists of 5, 4, 3, and 2 peaks. The closer the gate voltage is to a charge degeneracy point, the fewer nonequilibrium peaks can be observed. On the other hand, if the fine structure is due to a degenerate ground state, no highly excited states are involved, and the number of peaks in the multiplet is insensitive to V_g . Of course, both explanations (nonequilibrium processes and an almost degenerate ground state) can apply at the same time. In that case, multiple peaks will disappear at the same time, when V_g is tuned to the charge degeneracy point. An alternative way to distinguish between the two scenarios is if the parity of the number of electrons N can be changed by a gate voltage. Nonequilibrium processes cannot explain a fine structure of the first resonance if N is odd.

5 Conclusions

In this article, we have reviewed several effects related to the electrons' spin in the presence of spin-orbit coupling and/or electron–electron interaction, in small quantum dots with relatively large number of electrons.

At low temperatures, in the absence of spin-orbit coupling, and in the absence of an applied Zeeman field, our system can be described by an effective Hamiltonian of the form (1). In the limit where the number of electrons in a chaotic dot is large, the effective Hamiltonian contains three interaction parameters, in the direct, exchange and Cooper channels. In Appendices B and C we estimate these parameters for realistic systems. We have used them in Sec. 2 to calculate (i) the probability for the dot to have a non-zero total spin in its ground state and (ii) the distribution of the Coulomb blockade peak spacings. The theory for the latter describes many features of the experimental observations, and is qualitatively much better than what one would have obtained if one ignored the exchange interaction. However, the simple effective model does not do well in describing the low energy tail of the distribution, and it does not account for the large differences in the data obtained by different experimental groups.

In Sec. 3, we reviewed some recent theoretical studies on the effect of spin-orbit coupling in a quantum dot or metal particle. In Subsection 3.1 we discussed

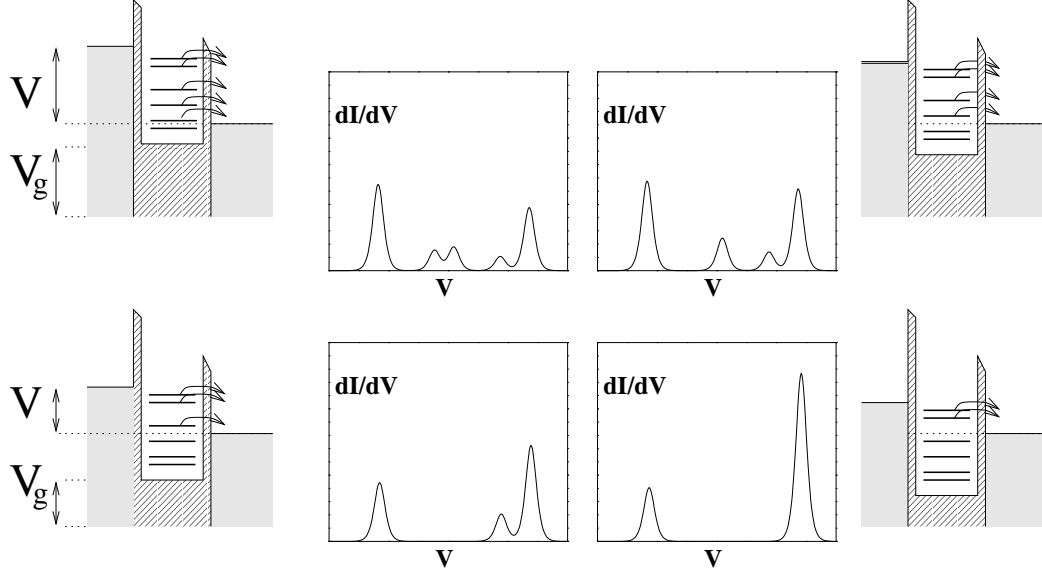


Fig. 14. When the voltage V_g of a nearby gate is varied, the number of excited N -particle states that can be populated by current flow is also changed. The four panels show how the peaks in the differential conductance disappear one by one when V_g is tuned in the direction of the charge-degeneracy point (at which current flow happens at zero bias voltage). As seen in the figure, the (minimal) bias voltage, V , for nonzero current flow decreases as V_g approaches the charge-degeneracy point. In the four panels shown, the number of peaks decreases from five (upper left) to two (lower right panel). The single-particle levels are for the $N + 1$ -particle system; the arrows indicate from which levels electrons can escape to the right reservoir. The dI/dV graphs were calculated using the rate equations of Refs. [5,34], with randomly chosen values for the interaction matrix elements that determine the dependence of transition energies on the precise population of the single-particle levels in the grain, see Subsection 2.1.1. The typical distance between the peaks is of order Δ/\sqrt{g} , where g is the dimensionless conductance of the metal grain.

the relation between the splitting of the ground state Kramers degeneracy (in the case of a strong spin-orbit coupling and a weak magnetic field) and an effective g -tensor. The joint probability distribution of the eigenvalues of the tensor was presented. Recent experiments [25] that measured the distribution of the g -tensor in particles of Cu, Ag, and Au, found good agreement with many aspects of the theoretical predictions.

The combined effects of spin-orbit coupling and electron-electron interactions were discussed in Subsection 3.2. It was argued that strong spin-orbit coupling will tend to inhibit the appearance of effects due to electron-electron interactions.

In Subsection 3.3, we reviewed how the peculiar form of the spin-orbit coupling for a two-dimensional electron system in a GaAs heterostructure of quantum well leads to a strong suppression of spin-orbit effects when the electrons are confined in a small quantum dot. We explained how a magnetic field, parallel

to a quantum dot in a AlGaAs 2DEG, enhances the weak spin-orbit effects in these dots. This observation may be used to tune the strength of spin-orbit coupling in quantum dots and may explain recent observations on fluctuations in the conductance through such dots.

We also discussed, in Subsection 4 possible explanations, based on non equilibrium phenomena, and an almost degenerate ground states due to spin-orbit coupling and electron-electron interaction, for the observations [4] of a multiplet splitting of the lowest resonance in the tunneling conductance through a gold nanoparticle.

A few recent developments in the young field of spin and interaction effects in small quantum systems have been examined in this article. At present, there is no quantitative theory that can explain all the experimental observations in this area. Current theories describe well several aspects of small dots (for example the g -tensor eigenvalue distribution), but in others aspects, such as Coulomb blockade peak spacing, the agreement between theory and experiment is far from being satisfactory.

6 Acknowledgments

It is our pleasure to thank our collaborators J. N. H. J. Cremers, Ady Stern, J. A. Folk and C. M. Marcus. Special thank are due to S. R. Patel and C. M. Marcus for allowing us using their data in this publication and for enlightening conversations. We also thank M. Tinkham and D. Davidovic for helpful discussions, and S. Lüscher, T. Heinzl and K. Ensslin for sending us their data. This work was supported at Harvard by NSF grants DMR-9809363 and DMR-9981283, at Cornell by NSF grant DMR-0086509 and by the Sloan Foundation, and at Weizmann by the German-Israeli Project Corporation DIP-c7.1.

A Derivation of the effective Hamiltonian [Eq. (1)] from the toy model with contact interaction [Eq. (2)]

In order to analyze the ground state energy for the toy model Hamiltonian (2), the electron-electron interaction is separated into mean and fluctuations,

$$\begin{aligned}
 uM \sum_m n_{m\uparrow} n_{m\downarrow}, &= uM \sum_m (\langle n_{m\uparrow} \rangle n_{m\downarrow} + n_{m\uparrow} \langle n_{m\downarrow} \rangle) \\
 &\quad + uM \sum_m \delta n_{m\uparrow} \delta n_{m\downarrow}
 \end{aligned}$$

$$- uM \sum_m \langle n_{m\uparrow} \rangle \langle n_{m\downarrow} \rangle, \quad (\text{A.1})$$

where $\delta n_{ms} = n_{ms} - \langle n_{ms} \rangle$ and the average occupation $\langle n_{m,\uparrow} \rangle = \langle n_{m,\downarrow} \rangle$ is calculated using the self-consistent (Hartree-Fock) Hamiltonian

$$\mathcal{H}^{\text{HF}} = \sum_{n,m,s} c_{n,s}^\dagger \mathcal{H}_0(n,m) c_{m,s} + uM \sum_m (\langle n_{m\uparrow} \rangle n_{m\downarrow} + n_{m\uparrow} \langle n_{m\downarrow} \rangle). \quad (\text{A.2})$$

For technical convenience, we define the occupancies $\langle n_{ms} \rangle$ in a reference state with $2N - 2K$ electrons and zero spin, where K is a number of order unity, chosen such that all relevant particle-hole excitations have energy less than $K\Delta$. For a disordered metal grain, we may assume that the eigenvectors and eigenvalues $\varepsilon_\mu^{\text{HF}}$ of \mathcal{H}^{HF} are distributed like those of a random matrix (with the possible exception of the spacing of two eigenvalues closest to the Fermi level, see Refs. [3,18]; a reference state with $2N - 2K$ electrons, rather than with $2N$ electrons is chosen, to ensure that only eigenvalues of \mathcal{H}^{HF} above the Fermi level are needed). The last term on the r.h.s. of Eq. (A.1) is a constant shift of the energy and can be omitted.

We then construct a state with $2N$ (or $2N + 1$) electrons by adding $2K$ (or $2K + 1$) electrons to the reference state, and find an effective Hamiltonian for low-lying particle-hole excitations using the remaining third term on the r.h.s. of Eq. (A.1) as a perturbation. The derivation of this effective Hamiltonian proceeds along the lines sketched in Sec. 2.2 and Ref. [2]. In the limit $M \rightarrow \infty$, the effective Hamiltonian has the form (1), where to lowest nontrivial order in u one has $\varepsilon_\mu = \varepsilon_\mu^{\text{HF}}$ and $-J_s = J_c = u$.

When studying the effective interaction amplitudes perturbatively in u , one finds that virtual particle-hole excitations involving states with energies ε far away from E_F ($\Delta < \varepsilon - E_F < E_{\text{Th}}$) contribute to the $O(u^2)$ term and to higher order terms. This leads to an effective renormalization of the interaction constants J_s and J_c , and of the spacing between the levels ε_μ . For example,

$$J_s(u) = u + u^2 \frac{1}{M} \left[\int_{E_F}^{E_F} d\varepsilon d\varepsilon' \frac{\nu(\varepsilon)\nu(\varepsilon')}{\varepsilon + \varepsilon'} - \int_{E_F} d\varepsilon d\varepsilon' \frac{\nu(\varepsilon)\nu(\varepsilon')}{\varepsilon + \varepsilon'} \right] + \mathcal{O}(u^3), \quad (\text{A.3})$$

$$\begin{aligned} \varepsilon_\mu(u) = \varepsilon_\mu^{\text{HF}} - u^2 \varepsilon_\mu^{\text{HF}} \frac{1}{M} & \left[\int_{E_F}^{E_F} d\varepsilon d\varepsilon' \int_{E_F} d\varepsilon'' \frac{\nu(\varepsilon)\nu(\varepsilon')\nu(\varepsilon'')}{(\varepsilon + \varepsilon' - \varepsilon'')^2} \right. \\ & \left. + \int_{E_F}^{E_F} d\varepsilon \int_{E_F} d\varepsilon' d\varepsilon'' \frac{\nu(\varepsilon)\nu(\varepsilon')\nu(\varepsilon'')}{(\varepsilon - \varepsilon' - \varepsilon'')^2} \right] + \mathcal{O}(u^3), \quad (\text{A.4}) \end{aligned}$$

where $\nu(\varepsilon)$ is the density of states for the Hamiltonian \mathcal{H}^{HF} , and J_c is renormalized to zero (see appendix C).

Beyond the first order in the interaction strength u , the symmetry of the effective Hamiltonian (1), and of the result (4) that was derived from it, differs from that of the equivalent expression in Ref. [3], which was obtained from the toy model (2) using the selfconsistent Hartree-Fock approximation. The reason of this difference is that, in higher orders of perturbation theory, the selfconsistent Hartree-Fock approximation neglects certain contributions to the ground state energy. (For example, the first correction to J_s is of second order in u [second term in Eq. (A.3)], and not, as in the Hartree-Fock approximation, of third order[3].)

When all contributions are taken into account, the symmetry of Eq. (4) and the form of the effective Hamiltonian (1) is preserved to all orders in u .

B The relation between the parameter $\lambda = -J_s/\Delta$ and \mathbf{r}_s

Landau-Fermi-liquid theory expresses various properties of the system in terms of the coefficients $f_{\rho\sigma\rho\sigma'}$. Using the notations of Ref. [35] we find:

$$\frac{C}{C_b} = \frac{m^*}{m_b} = 1 + \frac{F_1^s}{d}; \quad \frac{\chi_P}{\chi_{Pb}} = \frac{m^*}{m_b} \frac{1}{1 + F_0^a}, \quad (\text{B.1})$$

where C is the specific heat, χ_P the Pauli susceptibility. The quantities with the suffix $-_b$ include band effects, but do not include electron-electron interaction corrections. The latter are encompassed in the F -coefficients of the Landau Fermi liquid theory. The letter d denotes the dimension of the system. For ballistic systems there are no anomalous renormalizations of the Fermi-Liquid coefficients and we have:

$$\lambda = -J_s/\Delta = -F_0^a = 1 - \frac{\chi_P}{\chi_{Pb}} \frac{m^*}{m_b} = 1 - \frac{\chi_{Pb}}{\chi_P} \frac{C}{C_b}. \quad (\text{B.2})$$

Thus, in principle the ratio of the specific heat and the susceptibility gives the desired interaction parameter J_s .

B.1 Three dimensions

There are various ways to calculate theoretically the Landau F parameters, using different approximations for the electron-electron interaction. They var-

ied from a simple static RPA approximation to more complicated approaches like density functional theory. Ref. [36] reviews the subject.

The relevant parameter to describe the strength of the interaction effects is r_s , the ratio of the typical potential energy to the kinetic energy of electrons. In metals it is defined by:

$$\frac{4\pi}{3}r_s^3a_B^3 = \frac{1}{n}, \quad a_B = \frac{e^2m_b}{\hbar^2\epsilon4\pi\epsilon_0} \quad (\text{B.3})$$

where n is the density of electrons and a_B is the Bohr radius in the metal. Some values for r_s in metals are giving in Ref. [37] (page 74) and in Ref. [38].

For $0 < r_s < 5$ the effective mass[37] ranges between $0.96 < m^*/m_b < 1.06$ where for small r_s (< 3), $m^* < m_b$, and for larger r_s (> 3), $m^* > m_b$. (See table VII on page 103 in [37].)

Using the approximation of Rice [39] for the effective mass and for the susceptibility one can roughly approximate

$$\lambda_{\text{Rice}}(r_s) \sim (3 + r_s)/25, \text{ for } 1 < r_s < 5. \quad (\text{B.4})$$

Another approximation for the susceptibility is given in [36] see page 256. Assuming that the effective mass is renormalized as in the Rice approach (i.e. not very significant renormalization) we find that:

$$\lambda_{\text{Singwi}}(r_s) \sim (2 + r_s)/16, \text{ for } 1 < r_s < 5. \quad (\text{B.5})$$

For small $r_s \sim 1$ the difference between the estimations is only 15 % while for $r_s \sim 5$ it close to 30 %. The second estimate reproduces quite well experimental measurements of λ in a wide range of metals. The parameter λ is determined by various experimental methods such as electron spin resonance, spin wave, Knight shift and total susceptibility. [See p. 256 of Ref. [36] and reference therein for further details.]

Using Eqs. (B.4) and (B.5) we can estimate the parameter J_s in different materials; however the estimates are rough and should be taken with a grain of salt. Typical values for metallic elements are given in the table.

	Li	Na	K	Rb	Cs	Cu	Ag	Au
r_s	3.25	3.93	4.86	5.20	5.62	2.67	3.02	3.01
$\lambda_{\text{Rice}}(r_s)$	0.25	0.28	0.31	0.33	0.34	0.23	0.24	0.24
$\lambda_{\text{Singwi}}(r_s)$	0.33	0.37	0.43	0.45	0.48	0.29	0.31	0.31
	Be	Mg	Ca	Sr	Ba	Nb	Fe	Pb
r_s	1.87	2.66	3.27	3.57	3.71	3.07	2.12	2.30
$\lambda_{\text{Rice}}(r_s)$	0.19	0.23	0.25	0.26	0.27	0.24	0.20	0.21
$\lambda_{\text{Singwi}}(r_s)$	0.24	0.29	0.33	0.35	0.36	0.32	0.26	0.27

Table B.1 Estimations for $\lambda = -J_s/\Delta$ in selected metals.

B.2 Two dimensions

Most of the calculations for the Landau-Fermi-liquid parameters in two dimensional systems were performed for Silicon MOSFET. For a review see Ref. [36] (especially page 257) and Ref. [40] (pages 454 and 468).

We note that as we sweep an external magnetic field, perpendicular to the sample area, the spin susceptibility oscillates because the difference in the occupations of Landau levels with spins up and down. This effect makes the comparison between theory and experiment complicated. We will not be interested in such anomalously large exchange enhancement.

In case of silicon MOSFET we should include also the valley degeneracy, and the difference in the dielectric constants of Si and SiO that causes the dielectric function be space dependent. The screening from the metallic electrodes may influence the results as well.

For GaAs/AlGaAs heterostructures the first two complications are absent. It appears that due to the absence of valley degeneracy in GaAs/AlGaAs the parameter J_s should be larger than in the case of the Si MOSFET. Therefore, GA/AlGaAs might be more appropriate to the study of spin configurations and there dependance on interaction constants.

A static random phase approximation for GaAs gives [41]

$$\lambda = \frac{m^*}{m_b} G\left(\frac{r_s}{\sqrt{2}}\right); \quad G(x) = \begin{cases} \frac{x \operatorname{arccosh}(1/x)}{\pi \sqrt{1-x^2}} & \text{for } x \leq 1 \\ \frac{x \operatorname{arccos}(1/x)}{\pi \sqrt{x^2-1}} & \text{for } x > 1 \end{cases} \quad (\text{B.6})$$

where in two dimensions

$$r_s = \frac{e^2 m_b}{\hbar^2 \sqrt{\pi n} \epsilon 4\pi \epsilon_0} = \frac{5.45 * 10^5}{\sqrt{n(\text{cm}^2)}}. \quad (\text{B.7})$$

In the last equality we take $\epsilon = 12.9$, $m_b = 0.067m_e$ and m_e is the free electron mass.

It can be verified that

$$G(x) \xrightarrow{x \rightarrow \infty} 1/2 \quad \text{and} \quad G(x) \xrightarrow{x \rightarrow 0} (x/\pi) \log(2/x).$$

The factor $1/2$ for large x is due to the spin degeneracy and appears because both spins participate in the screening in the RPA approximation. (In case of a MOSFET the factor $1/2$ is substituted by $1/4$ due to the valley degeneracy.)

The same static RPA approximation gives for the effective mass:

$$m_b/m^* = 1 - (\sqrt{2}/\pi)r_s + r_s^2/2 + (1 - r_s^2)G(r_s/\sqrt{2}). \quad (\text{B.8})$$

Numerically, in this approximation $0.95 < m^*/m_b < 1$. In other words within the static RPA approximation the mass renormalization is not very significant.

Using this approximation we plot $-J_s$ as a function of r_s and n in Fig. B.1. For example, $\lambda(n = 0.7 * 10^{11} \text{cm}^{-2}) \cong \lambda(r_s \cong 2) \sim 0.34$,

C Renormalization of the interaction in the Cooper channel

In Sec. 2.1 we described how to integrate out the interaction between electrons at high frequency in the RG sense. The interaction in the Cooper channel deserves a special consideration, as we will see below it reduces substantially when the temperature decreases.

To see how it works in practice we look at the Dyson equation for the vertex part of the interaction in the Cooper channel (for a precise definition of the vertex part see Ref. [42] Sec. 33.3). Since the divergencies in the Cooper

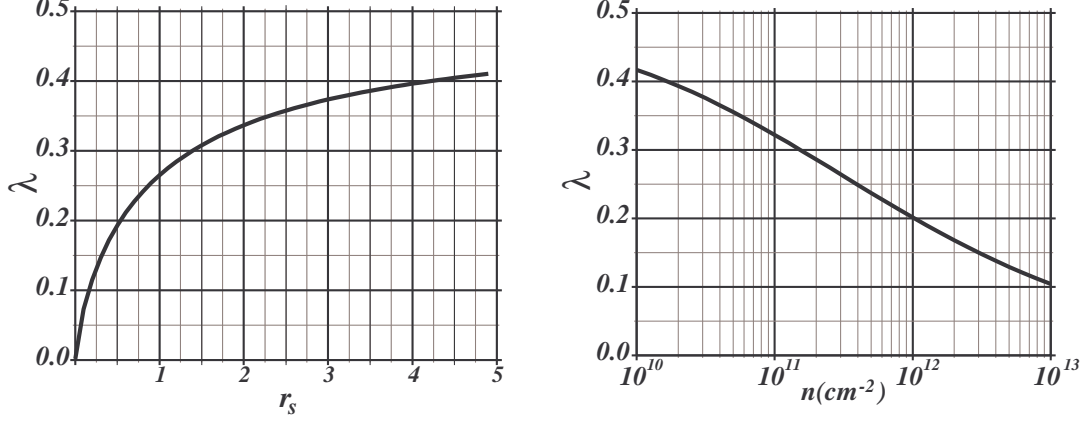


Fig. B.1. λ as a function of the ratio of the typical potential energy to the kinetic energy of electrons r_s , and as a function of the electron density n , for GaAs/AlGaAs heterostructures in the static RPA approximation.

channel are logarithmic we can write the Dyson equation, for T larger than the inverse of the elastic mean free time τ , in a RG form[16]:

$$dJ_c(T)/dl = -J_c^2(l)/\Delta, \quad l = \log(E_F/T), \quad T > 1/\tau. \quad (\text{C.1})$$

Integration of this equation, from E_F to T gives

$$J_c(T) = \frac{J_c(E_F)}{1 + (J_c(E_F)/\Delta) \log(E_F/T)}. \quad (\text{C.2})$$

This logarithmic suppression of the interaction in the Cooper channel was first discussed in Ref. [43] and is known as the Tolmachev-Anderson-Morel log or pseudo-electron-potential log.

In quasi-two-dimensional samples, for $T < 1/\tau$ the RG equation (C.1) is modified to [16]:

$$dJ_c(T)/dl = \Delta/(g\pi) - J_c^2(T)/\Delta, \quad 1/\tau > T > E_{\text{Th}}. \quad (\text{C.3})$$

We have neglected here the effects of the diffusive motion on the other channels. The presence of the term $1/(\pi g)$ slows down the logarithmic reduction in the Cooper channel, and physically describes the enhancement of the interaction between the electrons in the Cooper channel due to their diffusive motion. In case of quasi-one-dimensional systems the full Dyson equation should be solved[44].

Finally, the process of integration of the motion at high frequencies reaches the Thouless energy, and we find the effective Hamiltonian (1). We will analyze the Cooper channel for energies below the Thouless energy using the contact

model (2). In principle, the behavior of the Cooper channel can be solved exactly by the method of Richardson [45]. But, to understand qualitatively the reduction of the interaction in the Cooper channel, at energy below E_{Th} it is sufficient to solve the Dyson equation for the interaction matrix element $\langle \alpha \bar{\alpha} | \hat{u} | \alpha \bar{\alpha} \rangle$ in the Cooper channel. Formally this equation is:

$$\langle \alpha \bar{\alpha} | \hat{u} | \alpha \bar{\alpha} \rangle = \langle \alpha \bar{\alpha} | \hat{u}^0 | \alpha \bar{\alpha} \rangle - \sum_{\nu \neq \alpha} \frac{\langle \alpha \bar{\alpha} | \hat{u}^0 | \nu \bar{\nu} \rangle \langle \nu \bar{\nu} | \hat{u} | \alpha \bar{\alpha} \rangle}{|\varepsilon_\alpha - \varepsilon_\nu|}, \quad (\text{C.4})$$

with $\hat{u}^0 = uM c_{n,\uparrow}^\dagger c_{n,\downarrow}^\dagger c_{n,\downarrow} c_{n,\uparrow} \delta_{nm}$, $\hat{u} = c_{n,\uparrow}^\dagger c_{n,\downarrow}^\dagger u(n, m) c_{m,\downarrow} c_{m,\uparrow}$, the operator $\psi_{\alpha\uparrow(\downarrow)}^\dagger = \sum_{n=1}^M \phi_{\alpha\uparrow(\downarrow)}(n) c_{n,\uparrow(\downarrow)}^\dagger$ where the functions $\phi_\mu(n)$ are real eigenfunctions of a random matrix with real elements, n runs on the sites of the random systems, M is the total number of sites, and $|\alpha \bar{\alpha}\rangle = \psi_{\alpha\downarrow}^\dagger \psi_{\alpha\uparrow}^\dagger |0\rangle$. Using the anti-commutation relations of $c_{n,s}$ operators we find an equation for the unknown amplitudes $u(n, m)$

$$\begin{aligned} & \sum_{nm} \phi_\alpha^2(n) u(n, m) \phi_\alpha^2(m) = \\ & \sum_{nm} \phi_\alpha^2(n) (uM \delta_{nm}) \phi_\alpha^2(m) + \\ & \sum_{n,m,l,k,\nu \neq \alpha} \frac{\phi_\alpha^2(n) (uM \delta_{nl}) \phi_\nu^2(l) \phi_\nu^2(k) u(k, m) \psi_\alpha^2(m)}{\varepsilon_\alpha - \varepsilon_\nu}. \end{aligned} \quad (\text{C.5})$$

Now with the relation $\langle \phi_\mu^2(l) \phi_\mu^2(k) \rangle = 1/M^2 (1 + 2\delta_{lk})$ (that is valid in the limit $M \rightarrow \infty$) we find, comparing the elements in the series that sum over n and m

$$u(n, m) = uM \delta_{nm} - \lambda \frac{\log M}{M} \left(\sum_l u(l, m) + 2u(n, m) \right), \quad (\text{C.6})$$

where the logarithmic factor appears from the summation over the energies ν . The term $\propto 2u(n, m)$ on the left hand side can be neglected as it is small [by a factor $(\log M)/M$] compared to the one on the right hand side. A summation over n gives now

$$\sum_l u(l, m) = \frac{uM}{1 + \lambda \log M}$$

substituting in (C.6) and taking the limit $M \gg 1$ we find:

$$u(n, m) = \frac{M \delta_{nm} + \lambda \log M (M \delta_{nm} - 1)}{1 + \lambda \log M}, \quad (\text{C.7})$$

where $\lambda = u/\Delta$ and Δ is the average level spacing in the dot. Hence:

$$\langle \alpha \bar{\alpha} | \hat{u} | \alpha \bar{\alpha} \rangle = \frac{1}{M^2} \sum_{m,n} (1 + 2\delta_{nm}) u(n, m) = 2u + \frac{u}{1 + \lambda \log M}. \quad (\text{C.8})$$

The logarithmic factor reduces the term that is $\propto \frac{1}{M^2} \sum u(n, m)$ and does not involve the δ_{nm} factor. This term correspond to the Cooper channel as it involves contraction of two wave functions, associated with two creation (or two annihilation) operators. Thus, we find that from the Thouless energy up to energies of the order of the level spacing, similarly to the pseudo-electron-potential log [see after Eq. (C.2)], there is an additional logarithmic suppression of the interaction in the Cooper channel. For that reason we took $J_c = 0$ in the analysis of the ground state spin distributions in Sec. 2.2 and the Coulomb blockade peak spacing in Sec. 2.3.

References

- [1] L. L. Sohn, L. P. Kouwenhoven, and G. Schon, *Mesoscopic Electron Transport* (Kluvers, Dordrecht, 1997), nato ASI Series E 345.
- [2] I. L. Kurland, I. L. Aleiner, and B. L. Altshuler, Phys. Rev. B **62**, 14886 (2000).
- [3] P. W. Brouwer, Y. Oreg, and B. I. Halperin, Phys. Rev. B **60**, R13977 (1999).
- [4] D. Davidovic and M. Tinkham, Phys. Rev. B **61**, R16359 (2000).
- [5] C. W. J. Beenakker, Phys. Rev. B **44**, 1646 (1991). Y. Alhassid Rev. Mod. Phys. **72**, 895 (2000).
- [6] Y. Oreg, K. Byczuk, and B. I. Halperin, Phys. Rev. Lett. **85**, 365 (2000).
- [7] U. Sivan *et al.*, Phys. Rev. Lett. **77**, 1123 (1996).
- [8] F. Simmel, T. Heinzel, and D. A. Wharam, Euro. Lett. **38**, 123 (1997).
- [9] S. R. Patel *et al.*, Phys. Rev. Lett. **80**, 4522 (1998).
- [10] S. Lüscher *et al.*, Phys. Rev. Lett. **86**, 2118 (2001).
- [11] H. U. Baranger, D. Ullmo, and L. I. Glazman, Phys. Rev. B **61**, R2425 (2000).
- [12] D. Ullmo and H. U. Baranger, cond-mat/0103098, (2001).
- [13] I. L. Aleiner, P. W. Brouwer, and L. I. Glazman, cond-mat/0103008, (2001).
- [14] R. Shankar, Rev. Mod. Phys. **66**, 129 (1994).

- [15] J. Polchinski, Effective Field Theory and the Fermi Surface, Proceedings of 1992 Theoretical Advanced Studies Institute in Elementary Particle Physics, edited by J. Harvey and J. Polchinski (World Scientific, Singapore, 1993), 1993, hep-th/9210046.
- [16] A. M. Finkel'stein, in *Soviet Scientific Review*, edited by I. M. Khalatnikov (Harwood Academic Publisher GmbH, Moscow, 1990), Vol. 14.
- [17] R. Berkovits, Phys. Rev. Lett. **81**, 2128 (1998).
- [18] S. Levit and D. Orgad, Phys. Rev. B **60**, 5549 (1999).
- [19] Y. M. Blanter, A. D. Mirlin, and B. A. Muzykantskii, Phys. Rev. Lett. **78**, 2449 (1997).
- [20] Y. M. Blanter, Phys. Rev. B **54**, 12807 (1996), (See formula 42).
- [21] Y. M. Blanter, A. D. Mirlin, and B. A. Muzykantskii, Phys. Rev. Lett. **80**, 4161 (1998).
- [22] G. Usaj and H. U. Baranger, cond-mat/0108027, (2001).
- [23] K. A. Matveev, L. I. Glazman, and A. I. Larkin, Phys. Rev. Lett. **85**, 2789 (2000).
- [24] P. W. Brouwer, X. Waintal, and B. I. Halperin, Phys. Rev. Lett. **85**, 369 (2000).
- [25] J. R. Petta and D. C. Ralph, cond-mat/0106452, (2001).
- [26] B. I. Halperin *et al.*, Phys. Rev. Lett. **86**, 2106 (2001).
- [27] J. A. Folk *et al.*, Phys. Rev. Lett. **86**, 2102 (2001).
- [28] I. L. Aleiner and V. I. Fal'ko, cond-mat/0107385, (2001).
- [29] J. S. Meyer, A. Altland, and B. L. Alt'shuler, cond-mat/0105623, (2001).
- [30] V. I. Fal'ko and T. Jungwirth, cond-mat/0106019, (2001).
- [31] O. Agam *et al.*, Phys. Rev. Lett. **78**, 1956 (1997).
- [32] J. von Delft and D. C. Ralph, Phys. Rep., to be published.
- [33] O. Agam and I. L. Aleiner, Phys. Rev. B **56**, R5759 (1997).
- [34] D. V. Averin, A. N. Korotkov, and K. K. Likharev, Phys. Rev. B **44**, 6199 (1991).
- [35] D. Pines and P. Nozières, *The theory of quantum liquids* (W .A. Benjamin Inc, New York, 1966).
- [36] K. S. Singwi and M. P. Tosi, Sol. Stat. Phys. **36**, 177 (1981).
- [37] L. Hedin and S. Lundqvist, Sol. Stat. Phys. **23**, 1 (1969).
- [38] N. W. Ashcroft, *Solid State Physics* (CBS publishing Asia Ltd., Philadelphia, 1987).

- [39] T. M. Rice, *Ann. Phys.* **31**, 100 (1965).
- [40] T. Ando, A. B. Fowler, and F. Stern, *Rev. Mod. Phys.* **54**, 437 (1982).
- [41] J. F. Janak, *Phys. Rev.* **178**, 1416 (1969). Notice that there is a mistake in the way that the valley degeneracy is introduced.
- [42] A. A. Abrikosov, L. P. Gorkov, and I. E. Dzyaloshinski, in *Methods of Quantum Field Theory in Statistical Physics*, edited by R. A. Silverman (Prentice-Hall, Inc. Englewood Cliffs, New-Jersey, 1963).
- [43] P. Morel and P. W. Anderson, *Phys. Rev.* **125**, 1263 (1962).
- [44] Y. Oreg and A. M. Finkel'stein, *Phys. Rev. Lett.* **83**, 191 (1999).
- [45] J. von Delft, *Annalen der Physik (Leipzig)* **10**, 219 (2001).